Chapter 3 Examination of a Strong Motion Velocity Instrument

3.1 Introduction

This report documents the investigation into the performance of the tri-axial VSE-355G2 Strong Motion Velocity Seismometer, purchased with IRIS funds in late 2001. The instrument is manufactured by Tokyo Sokushin Co. Ltd., Office 2-22-9, Nishi-Nipporim Arakawa-Ku, Tokyo, 116-0013 Japan (`www.to-soku.co.jp`). Photographs of the instrument are in Figure 3.1.

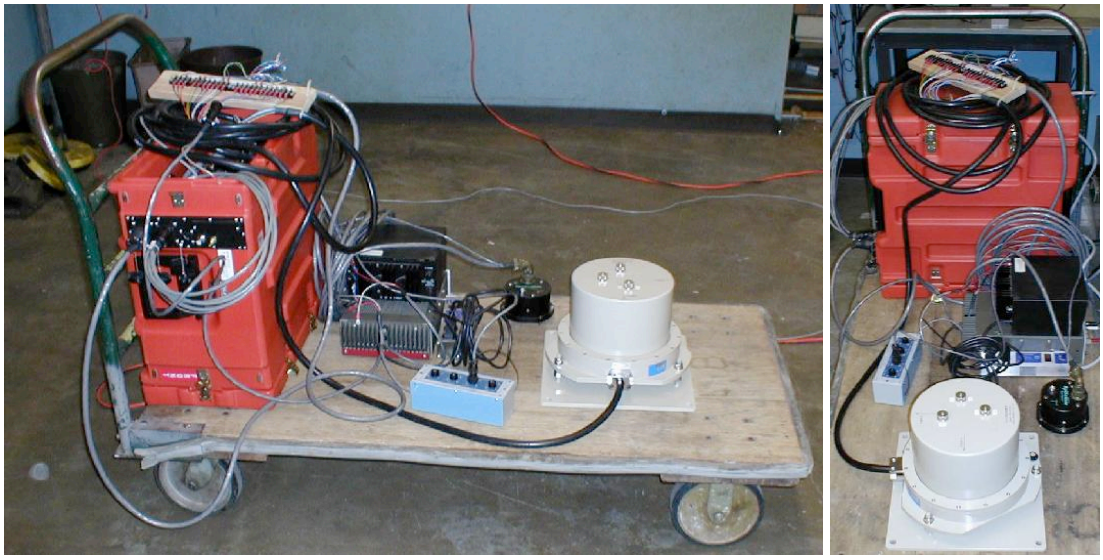

(a) Side view (b) Front view

Figure 3.1: VSE photo - Cart Test setup. VSE-355G2 is the large silver cylindrical instrument at the front of the cart, the EpiSensor is the small black cylindrical instrument just behind the VSE in the middle of the cart. A Q4120 datalogger (large rectangular box) is located at the back of the cart.

The instrument measures velocity as the standard output, from a heavily over-damped

mechanical pendulum and a feedback loop proportional to the pendulum displacement. A built-in calibration coil can provide known acceleration input for determination of the instrument sensitivity and frequency characteristics.

The performance of the instrument was determined by

- comparing earthquake signals and noise levels from the VSE-355G2 and a Streckeisen STS-2, co-located with the seismometer, in order to calibrate and obtain the sensitivity of the instrument.
- determining the system response to a known input, through the calibration coil, in order to estimate the equivalent SDOF instrument response.
- placing the instrument alongside an accelerometer on a laboratory cart and running the cart along the floor, in order to determine the actual instrument clip level (setup as in Figure 3.1).

A major design error was discovered during the original testing regime, the instrument was found to 'clip', or undergo non-linear behaviour, at velocities of only $15 cm/s$, significantly below the advertised clip level of $200 cm/s$ and also well below the expected velocities during large earthquakes. Exhaustive consultation and re-testing, involving many on-site visits from Tokyo-Sokushin, as well as independent tests carried out both here in the US and Japan, followed the discovery. A chronological list of the tests performed on the instrument are contained in Appendix A.

To obtain a satisfactory result from the cart tests which determine a broadband clipping level, the manufacturer had to replace and redesign the feedback and the suspension of the instrument. Once it had been established the instrument performed to the initial specifications in terms of strong motion recording, in late 2003, all the initial tests performed in 2001/2002 were repeated again with the new instrument. After the overhaul, the manufacturer changed the name from the VSE-355G2 to the VSE-355G3. The overhaul does change the characteristic response of the instrument somewhat, though it is still designed, and is in compliance with, the original specifications.

Results and background discussion relating to the instrument performance in general, and the results from the initial set of tests comprise this Chapter. Chapter 4 presents an analysis of the performance of the VSE-355G2 during the M8.3 Tokachi-Oki earthquake. The results of the tests on the VSE-355G3 are presented in Chapter 5.

The VSE-355G2 instrument, as received in 2001, has been operational in Japan for a number of years. It has been deployed at a number of stations (> 45) as the strong motion sensor in conjunction with an STS-2 (or similar) seismometer in the Freesia Broadband Seismic Network, or F-Net [`www.fnet.bosai.go.jp`]. The VSE-355G, an earlier version of the VSE-355G2, comprises the rest of the strong motion sensors (~ 80 stations in total). The manufacturer also has these and other strong motion velocity-meters deployed in other networks around Japan, which do not freely distribute their data. Data from F-Net shows the ability of the instrument to resolve motions beyond even hundreds of seconds from large teleseismic events. Data from the M8.3 23 September 2003 Tokachi-Oki earthquake off Hokkaido Island is analysed in Chapter 4, which shows how existing instruments in the network also perform poorly when motions reach over $15 cm/s$.

The instrument is currently deployed alongside a Guralp CMG-1T at California Integrated Seismic Network (CISN) station CRP, the Robinson Pit at Caltech. The planned longterm deployment for the instrument is at a new 3-channel CISN Station, within $1/2$ a kilometre of the existing TriNet Station SVD near San Bernadino, in close proximity to the San Andreas Fault.

3.2 A Note on Removing the Instrument Response

The problem of removing the instrument response from data is often ignored if the frequency band of interest is inside a region of flat response of the seismometer. In this case the record in counts (as output by the datalogger) is simply divided by the station gain, giving the ground acceleration (for an accelerometer) or ground velocity (for a typical broadband sensor or strong motion velocity-meter). The station gain, G, is determined from the sensitivity, or gain, of the sensor (G_s), and the gain of the datalogger (G_d). Table 3.1 gives some typical examples.

Sensor	G_s	**Datalogger**	G_d *(cts/Volt)*	**Station Gain, G**
STS-2	$1500V/m/s$	Q4120	$2^{23}/20$	$6,291,456cts/cm/s$
STS-2	$1500V/m/s$	Q730	$2^{23}/16$	$7,864,320cts/cm/s$
STS-1	$2500V/m/s$	Q4120	$2^{23}/20$	$10,485,760cts/cm/s$
STS-1	$2500V/m/s$	Q730	$2^{23}/16$	$13,107,200cts/cm/s$
EpiSensor	$10V/g$	Q4120	$2^{23}/20$	$4,275.5cts/cm/s^2$
EpiSensor	$10V/g$	Q730	$2^{23}/16$	$5,344.4cts/cm/s^2$
FBA-23	$5V/g$	Q4120	$2^{23}/20$	$2,137.8cts/cm/s^2$
FBA-23	$5V/g$	Q730	$2^{23}/16$	$2,672.2cts/cm/s^2$
FBA-23	$5V/g$	K2	$2^{18}/1.5$	$890.7cts/cm/s^2$
VSE-355G2	$10V/m/s$	Q4120	$2^{23}/20$	$41,943.0cts/cm/s$
VSE-355G2	$10V/m/s$	Q730	$2^{23}/16$	$54,428.8cts/cm/s$

Table 3.1: Typical Station Gains

Gains for some other instruments and dataloggers, as well as the frequency ranges for which the sensors have flat response, can be found in Tables 2.1 and 2.2.

Following Kanamori (2002) and Heaton (2003), the equation of motion for a simple seismometer is

$$\ddot{x}(t) + 2\beta\dot{x}(t) + \omega_0^2 x(t) = G\ddot{u}(t) \tag{3.1}$$

where $x(t)$ is the displacement response of the seismometer,

$u(t)$ is the displacement of the ground,

ω_0 is the natural frequency of the seismometer, *radians*,

$\omega_0 = 2\pi f$, f is the natural frequency of the seismometer, Hz,

$\beta = 2\zeta\omega_0$, ζ is the damping ratio.

In this case, the frequency response of the instrument to ground motion displacement, I_d, is found by taking the Fourier Transform of Equation 3.1:

$$I_d(\omega) = \frac{X(\omega)}{U(\omega)} = \frac{G\omega^2}{\omega^2 - 2i\beta\omega_0\omega - \omega_0^2} \tag{3.2}$$

or, in terms of frequency, f:

$$I_d(f) = \frac{X(f)}{U(f)} = \frac{Gf^2}{f^2 - 2i\beta f_0 f - f_0^2} \tag{3.3}$$

In this case, the response of the instrument when $f > f_0$ is $I_d(f) \approx G$, so is flat to displacement.

Accelerometer: Similarly, the frequency response of the instrument to ground motion acceleration, I_a, can be expressed as:

$$I_a(f) = \frac{X(f)}{-f^2 U(f)} = \frac{-G}{f^2 - 2i\beta f_0 f - f_0^2} \tag{3.4}$$

In this case, the response of the instrument when $f < f_0$ is $I_d(f) \approx G/f_0^2$, so is flat to acceleration. This is the case of the typical accelerometer. The natural frequency, f_0 of modern accelerometers is usually $50Hz$ or greater. This frequency is above the maximum frequency of interest in many cases in seismology and engineering, and is above the range of interest in this work. Thus, for accelerometer records with frequencies ranging from $50Hz$ to DC (or static offset), simple removal of the station gain is all the instrument correction that is required to obtain acceleration. This is illustrated by Figures 3.5 — 3.10 in the next Section. The ground displacement $u(t)$ as determined from the accelerometer output, $x(t)$, is then:

$$u(t) = \iint x(t)\, dt^2 + At + B \tag{3.5}$$

The initial conditions at time $t = 0$ are $u(0) = \dot{u}(0) = 0$ and $x(0) = \dot{x}(0) = 0$ (both ground and instrument response displacements and velocities are zero), so solving for the 2 constants of integration, $A = B = 0$. This is valid as long as pre-event noise is recorded by the datalogger, and this noise is significantly below the signal strength, a satisfactory assumption for large dynamic range stations in all but the noisiest locations for a wide range of ground motions.

The displacement derived from accelerometers is often unstable at long periods, as a double integration is required. Accelerations at long periods are very small, so the signal to noise is not good. Further, any small errors in the initial condition assumption that velocity and displacement are zero in the sensor timeseries cause large errors in the resultant displacement.

Even worse is the problem of bias in the initial baseline of acceleration:

$$\ddot{u}(t) = x(t) + C + Dt \tag{3.6}$$

where C is a baseline shift, and D is a linear trend.

The constants C and D can be very small, but are also double integrated:

$$u(t) = \iint x(t)\,dt^2 + Dt^3/3 + Ct^2/2 + At + B \tag{3.7}$$

So as time grows, a small baseline error will grow as a cubic or quadratic time-function. A baseline shift even of the order of the count level of the datalogger will cause instability with increasing time.

Strong Motion Velocity Meter: For the typical broadband instrument, such as the STS-2 and the VSE-355G2, the output can be modelled as a simple near critically damped oscillator with differential feedback. Thus the final output $y(t) = \dot{x}(t)$, and Equation 3.1 becomes:

$$\ddot{y}(t) + 2\beta\dot{y}(t) + \omega_0^2 y(t) = G\ddot{u}(t) \tag{3.8}$$

The frequency response of the instrument to ground motion velocity, I_v, is:

$$I_v(f) = \frac{Y(f)}{ifU(f)} = \frac{Gf^2}{f^2 - 2i\beta f_0 f - f_0^2} \tag{3.9}$$

So in this case, when $f > f_0$, $I_v(f) \approx G$, so the output is flat to velocity. The natural frequency of broadband instruments ranges from about $56s$ for the VSE-355EI to $360s$ for the STS-1 and CMG-1T. So for all signals with frequency content greater than f_0, removal of the instrument gain is all the processing required. (In reality there is also a corner at high frequencies, dependent on the instruments, but as the main interest is in recovering ground displacements, not high frequency accelerations, this is ignored here.) In the near-field of large earthquakes, static offsets are an expected occurrence, which have an infinite, or DC frequency that is important to measure. To recover this part of the waveform requires

removal of the instrument response.

There are many methods to remove the instrument response over the entire frequency range. The most complete method is to remove individual poles and zeros as determined from the sensor transfer function and other decimation / filtering operations performed by the feedback and A/D conversions of the datalogger (Scherbaum, 2001). This is because the manufacturers of the dataloggers include other complexities like anti-alias filters. These poles and zeros are described in the SEED files that are associated with some data-sets. As these are not available for all data-sets, two simple methods are described here. Both assume the sensor operates as a simple single degree of freedom (SDOF) seismometer, which is fully described by a gain factor, damping (ζ) and corner or natural frequency (f_0). For an SDOF, at the corner frequency, there are 2 poles corresponding to a change in slope in the frequency domain of $12dB/octave$. An example for the VSE-355G2, with corner at $93.2s$, is in Figure 3.13.

The two methods are (i) time domain solution (ii) frequency domain solution:

3.2.1 Time Domain Deconvolution: Direct Integration

Re-stating Equation 3.8

$$\ddot{y}(t) + 2\beta\dot{y}(t) + \omega_0^2 y(t) = G\ddot{u}(t) \tag{3.10}$$

Directly integrating, and summing all the constants, gives:

$$\dot{y}(t) + 2\beta y(t) + \omega_0^2 \int y(t)\,dt - A = G\ddot{u}(t) \tag{3.11}$$

Integrating two more times to get ground displacement, $u(t)$:

$$u(t) = \frac{1}{G}\left(\int y(t)\,dt + 2\beta \iint y(t)\,dt^2 + \omega_0^2 \iiint y(t)\,dt^3\right) - At^2/2 - Bt - C \tag{3.12}$$

For the initial conditions at time $t = 0$, assume that the seismometer response ($\dot{y}(0)$, $y(0)$, $\int y(t)\,dt\big|_{t=0}$, $\iint y(t)\,dt^2\big|_{t=0}$ and $\iiint y(t)\,dt^3\big|_{t=0}$) as well as the ground ($\dot{u}(0)$ and $u(0)$)

are at rest at the start of the record. As for the accelerometer, this is physically correct if the record contains pre-event noise, from a station with continuous data recording, or for a triggered station with a pre-trigger buffer. Again, poor signal-to-noise ratio in a record may introduce some error here:

$$u(t) = \frac{1}{G}\left(\int y(t)\,dt + 2\beta \iint y(t)\,dt^2 + \omega_0^2 \iiint y(t)\,dt^3\right) \tag{3.13}$$

Thus, instead of just removing the gain and integrating the output from the broadband instrument, $y(t)$, two extra terms involving the integral and double integral of the seismometer displacement $x(t)$ (recall $y(t) = \dot{x}(t)$) are required to get the deconvolved timeseries. The constants 2β and ω^2, on which the magnitude of these integral terms depend, are dependent on the equivalent SDOF each sensor best approximates, and so are sensor dependent. Table 3.2 shows the instrument constants derived from the appropriate SDOF for the commonly used broadband instruments analysed in this work. For an STS-1, with very long equivalent free period, the constants are small: $2\beta = 0.02468/s$ and $\omega_0^2 = 0.0003046 rad/s^2$ but for the VSE-355EI, with a relatively short free period of $T_0 = 56s$, the constants are an order of magnitude larger. Clearly as the natural frequency becomes higher, the proportion of the deconvolved signal due to the higher-order integrals increases. Nonetheless, even for the STS-1, as the length of the timeseries becomes longer, the deconvolved signal becomes more unstable.

Sensor	T_0 *(s)*	ζ *(%)*	2β $(1/s)$	ω_0^2 (rad/s^2)
VSE-355EI	56	65	0.1459	0.01259
VSE-355G	80	65	0.1021	0.006169
VSE-355G2	80	65	0.1021	0.006169
VSE-355G2 *	93.5	65	0.0836	0.004516
VSE-355G3	80	65	0.1021	0.006169
VSE-355G3 *	105.5	60	0.07147	0.003547
STS-2	120	70.7	0.07404	0.002742
STS-1	360	70.7	0.02468	0.0003046
CMG-1T	360	70.7	0.02468	0.0003046

Table 3.2: Typical broadband sensor constants, based on equivalent SDOF dynamic characteristics. * indicates equivalent SDOF as determined from laboratory testing.

This method is ideal for deconvolving the instrument response from transient signal like a large earthquake, which may record permanent ground displacements. Though the DC offset is not recorded by the sensor, it can be closely approximated as long as the permanent offset occurs within a short time. This is shown in Figure 3.2, which presents 3 components of data from a station 257km from the epicenter of the 25 September 2003 M8.3 Tokachi-Oki earthquake. Nearby GPS data indicates lateral offsets of $10cm$ EW and $-5cm$ NS, and $-2cm$ vertical offset. It is shown using the integration scheme of Equation 3.13, assuming zero initial conditions, gives static offsets similar the GPS. The 'raw' displacement does not include any static offset component.

As the initial velocities, displacements, and integrals of displacements are in fact known (in a band limited sense), these initial conditions could possibly be used to reduce error:

$$A = \dot{y}(0) + 2\beta y(0) + \omega_0^2 \int y(t)\,dt\Big|_{t=0} \tag{3.14}$$

$$B = y(0) + 2\beta \int y(t)\,dt\Big|_{t=0} + \omega_0^2 \iint y(t)\,dt^2\Big|_{t=0} \tag{3.15}$$

$$C = \int y(t)\,dt\Big|_{t=0} + 2\beta \iint y(t)\,dt^2\Big|_{t=0} + \omega_0^2 \iiint y(t)\,dt^3\Big|_{t=0} \tag{3.16}$$

So a more complete solution uses Equation 3.12 where the constants are defined in Equations 3.14, 3.15 and 3.16.

In Figure 3.2 data representing the integration using the initial conditions, Equation 3.12, are also included. This form is observed to lead to instability in 2 of the 3 components, without any improvement on the other component. This is because the sampling rate is $100sps$, and so any small changes in the count level of the first 2 elements of the timeseries lead to non-physically large accelerations once differentiated, and so constant A in Equation 3.12 becomes large. Decimation of the data, and tapering of the initial conditions, caused the resultant displacements to converge to the form from Equation 3.13, without any improvement in the longterm stability of the solution. As this method involves ad-hoc judgments about the character of the initial conditions themselves, henceforth time domain deconvolutions will only use the zero initial condition form of Equation 3.13.

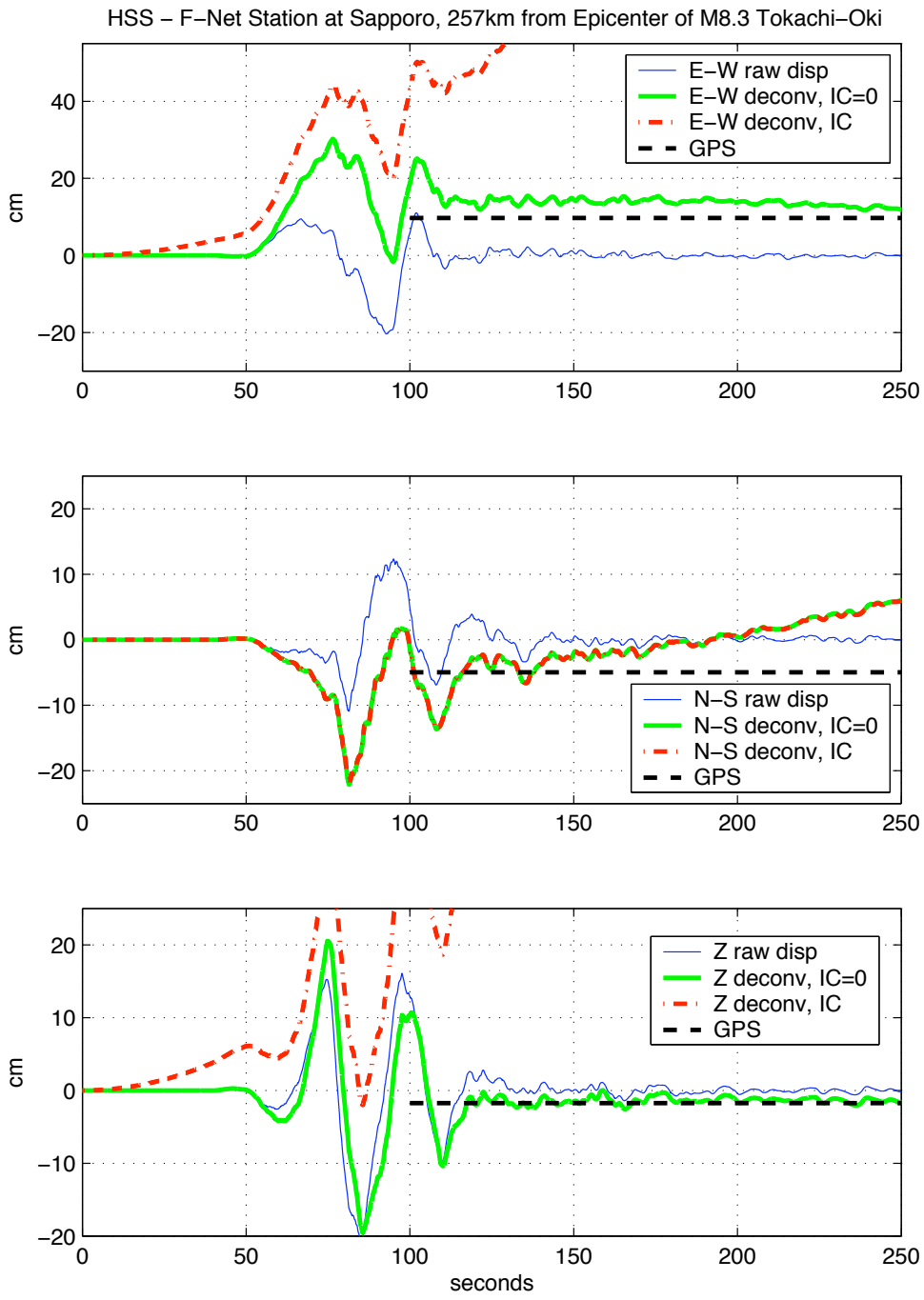

Figure 3.2: Time domain deconvolution of a strong motion record. VSE-355G2 at Station HSS, Sapporo town, 257km from epicenter of M8.3 Tokachi-Oki earthquake. Nearby GPS Station SAPPORO provides expected permanent offsets. 'Raw' displacement, simply gain removed and integrated raw VSE output, is observed to have zero static offset, contrary to the GPS data. Deconvolution using integration scheme of Equation 3.13, with zero IC's, gives best results. Using the initial conditions given in Equation 3.12 leads to instabilities.

3.2.2 Frequency Domain Deconvolution, Division by the Instrument Response

Another way of expressing the response of a single degree of freedom oscillator, $x(t)$, is as a convolution of the ground motion, $u(t)$, and the impulse response of the oscillator, $G(t)$:

$$x(t) = \ddot{u}(t) * G(t) \tag{3.17}$$

The convolution operator in the time-domain is equivalent to multiplication in the frequency domain:

$$X(\omega) = -\omega^2 U(\omega) G(\omega) \tag{3.18}$$

So the ground displacement, $u(t)$, can be found by an inverse FFT of $X(\omega)/[G(\omega).\omega^2]$.

This method is useful for very long timeseries, especially when analysing the noise content of a signal, or teleseismic waves. For strong motions with possible static offsets, it is unsatisfactory. To prevent numerical instabilities in the frequency domain division step, a low frequency cutoff must be chosen. Even if this cutoff is at a very long period, this will remove the static offset. This is illustrated in Figure 3.3.

In Figure 3.4 data is presented from the M6.5 San Simeon earthquake, 22 December 2003, as observed at Caltech CRP on a VSE-355G3. A 15*min* period from the E-W component is analysed, and the data is deconvolved using the two techniques described here. In this instance, though both the deconvolution appear stable in velocity even after 15*mins* (though the time-domain deconvolved velocity has a small static offset), the displacement records exhibit long period wandering, which produces different long period behaviour as seen in the FFT of the signals. High frequency behaviour is also attenuated in the the time domain method, likely because the deconvolution provides displacement at 1*sps*, which does not contain all the high frequency energy of 1*sps* velocity.

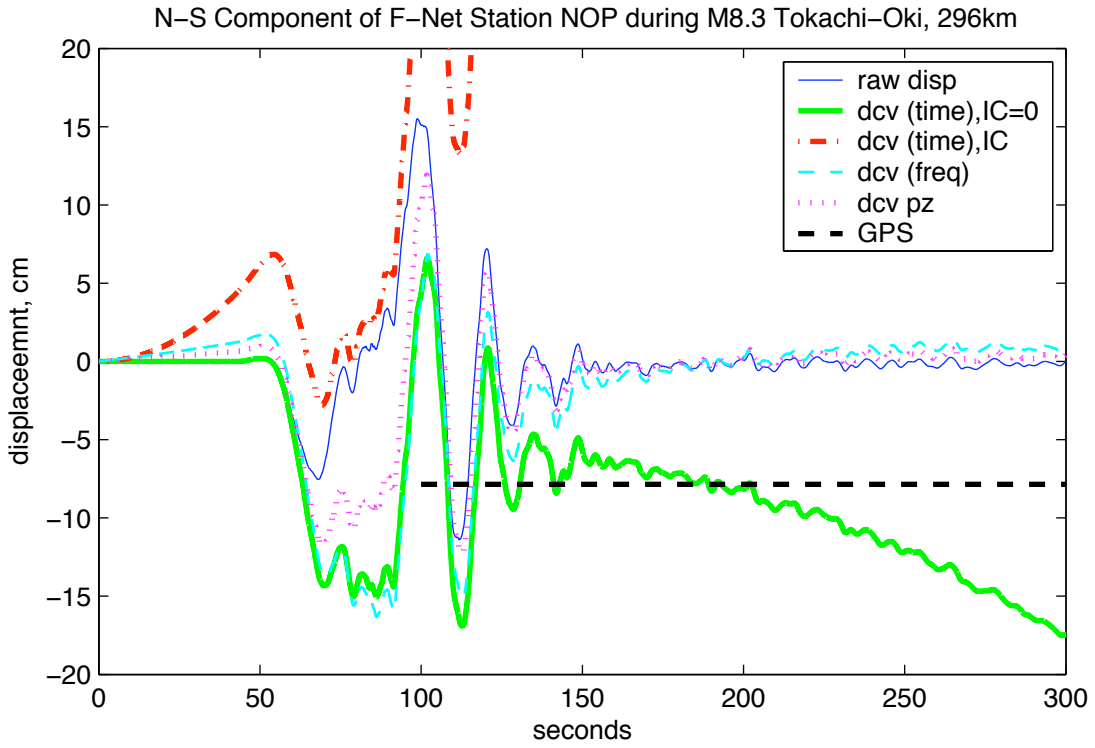

Figure 3.3: Comparison of time and frequency domain deconvolution for a strong motion record. VSE-355G2 at Station NOP, 296km from epicenter of M8.3 Tokachi-Oki earthquake. Nearby GPS Station TAKINOUE provides expected permanent offset of $-8cm$ ($8cm$ south). 'Raw' displacement, simply gain removed and integrated raw VSE output, shown to have zero static offset. Time domain deconvolution using integration scheme of Equation 3.13, with zero IC's, gives best results, with good correlation with GPS, though timeseries becomes instable after $160s$. Using the initial conditions in the time domain (Equation 3.12) leads to instabilities. Frequency domain deconvolutions, using both the SEED pole-zeros and the equivalent SDOF instrument response, approximate the deconvolved time domain response, but both produce no static offset.

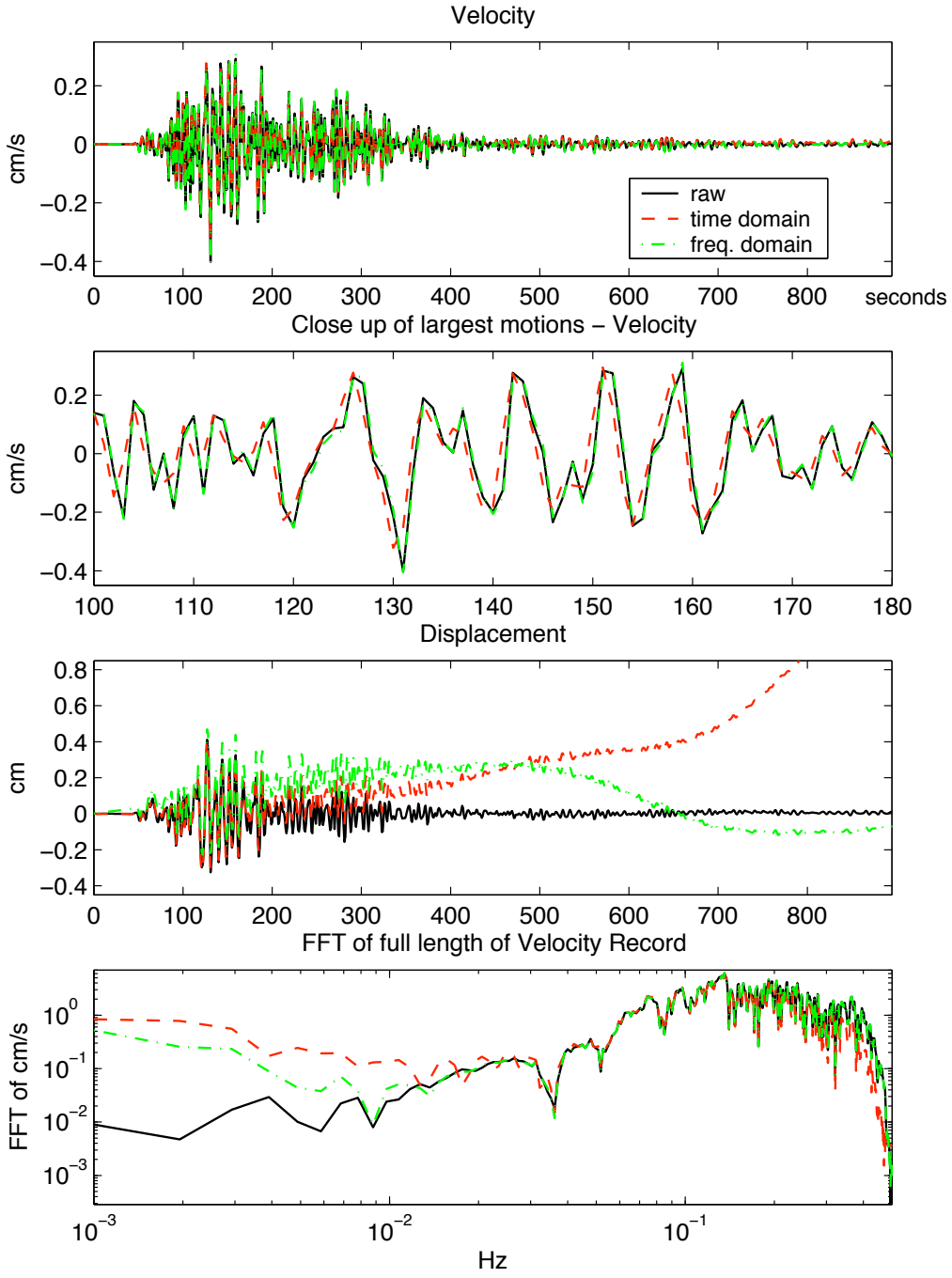

Figure 3.4: Time and frequency domain deconvolution comparison for regional motions: M6.5 San Simeon earthquake, 22 December 2003, at CRP, 323*km* distant. Recorded on a VSE-355G3. 15*min* of data from E-W component, comparing raw output (with pre-event mean and instrument gain removed), with the same output with a time domain deconvolution and a frequency domain deconvolution. Note from the FFT, the time domain deconvolution differs considerably at low frequencies, due to effect of offset at end of timeseries (Figure 3.4), and also has attenuation of high frequencies close to the Nyquist at 0.5*Hz*.

3.3 Synthetic Responses for the VSE-355G2 and FBA-23

In the course of this and the next two Chapters, the response of the various instruments to many different types of input motions is investigated. These inputs are in the form of controlled calibration coil voltages, laboratory tests of simplified, yet typical ground motions expected in large earthquakes, and actual ground motions. In this section, the synthetic output of the VSE-355G2 and the FBA-23, typical and representative of both strong motion velocity sensors, and accelerometers, are produced. It will be demonstrated that in the ideal case, both sensors can reproduce the input motions.

A given ground motion synthetic is generated, then convolved with the equivalent SDOF response that best approximates the seismometer. The FBA-23 SDOF is $f_0 = 50Hz, \zeta = 0.707$, and the VSE-355G2 SDOF is $T_0 = 94s$ and $\zeta = 0.65$. Deconvolutions using time domain integration are provided for the VSE.

Figures 3.5—3.10 present the 3 components of ground motion data, the FBA response, the VSE response, and the deconvolved VSE response, to the idealised ground motions. The FBA response is always multiplied by ω_0^2, following Equation 3.4, to account for the gain correction. The raw output from the accelerometer is shown as the acceleration timeseries for the FBA in all the Figures. It is noted this is nearly identical to the ground motion acceleration input, and deviates only at high frequencies approaching and above the $50Hz$ corner frequency. The VSE output is proportional to input ground velocity over a wide frequency band, but as these sample inputs all contain discontinuities and static offset, there are static frequency components of the motion which are not recorded by the raw VSE output, and thus the VSE output is not similar to the ground input velocity. The instrument response is then deconvolved from all of the raw VSE displacement timeseries by the time-domain direct integration method described by Equation 3.13. For these idealised ground motions, with no background noise, zero initial conditions, no instrument malfunction, and no tilting, the integration scheme produces the exact response.

All synthetics are generated using the SAC2000 'FUNCGEN' command, with $0.005Hz$ sampling frequency (200 samples per second). δ-functions are one time step only. All 'events' begin at $20s$. High amplitude, high frequency vibrations after the 'event' is finished

in the deconvolved VSE acceleration timeseries are not physical.

The synthetic ground motions investigated are —

1. δ-function in acceleration (*Figure 3.5*). This is a typical calibration coil input, and will be seen again in this Chapter, and Chapter 5.

2. step-function in acceleration (*Figure 3.6*). This is another typical calibration coil input, and will be seen again in this Chapter, and Chapter 5. This function is also produced as an error in certain accelerometers during strong, and sometimes even ambient, ground motions (Iwan et al, 1985). This step-function is also the response of an inertial sensor to a sudden tilt of the ground. Both the VSE and the FBA displacements are affected by this phenomenon. As can be seen in the Figure, resultant displacements will very strongly influenced by a small offset in acceleration. In Chapter 1, it is noted that a tilt of only $1\mu rad$ will produce an offset of $5cm$ in displacement after $100s$. In the laboratory experiments, this property of the response is used in calibration of the VSE, independent of the calibration coil — by adjusting the levelling screws, a tilt is imparted to the instrument, causing the response seen by the VSE. Modelling this output constrains the actual SDOF parameters of the VSE, a physical compliment to the calibration coil test.

3. ramp in acceleration, with static offset (*Figure 3.7*). A linear ramp, starting at $20s$ and lasting $5s$, causes a static offset of $0.1cm/s^2$. This is a more physically realistic model for a ground tilt, as it is not instantaneous, though the actual instrument responses are very similar to Figure 3.6, the step function in acceleration. Many examples of this motion will be seen in timeseries from the M8.3 Tokachi-Oki earthquake, in Chapter 4.

4. step in displacement (*Figure 3.8*). A static offset in displacement is modelled. This is a model for instrument response to ground deformation without measurable tilt, such as may occur in lateral spreading, or a tectonic co-seismic slip.

5. ramp in displacement, with static offset (*Figure 3.9*). A linear ramp lasting $5s$ from starting at $20s$ causes a static offset in displacement of $20cm$. This is equivalent to 2 equal and opposite δ-functions, the first positive at $20s$, , the second negative at $25s$, in acceleration. This is a more physically realistic model for a ground deformation, though the actual instrument responses are very similar to Figure 3.8, the step function in acceleration. Examples of this will also be seen in Chapter 4.

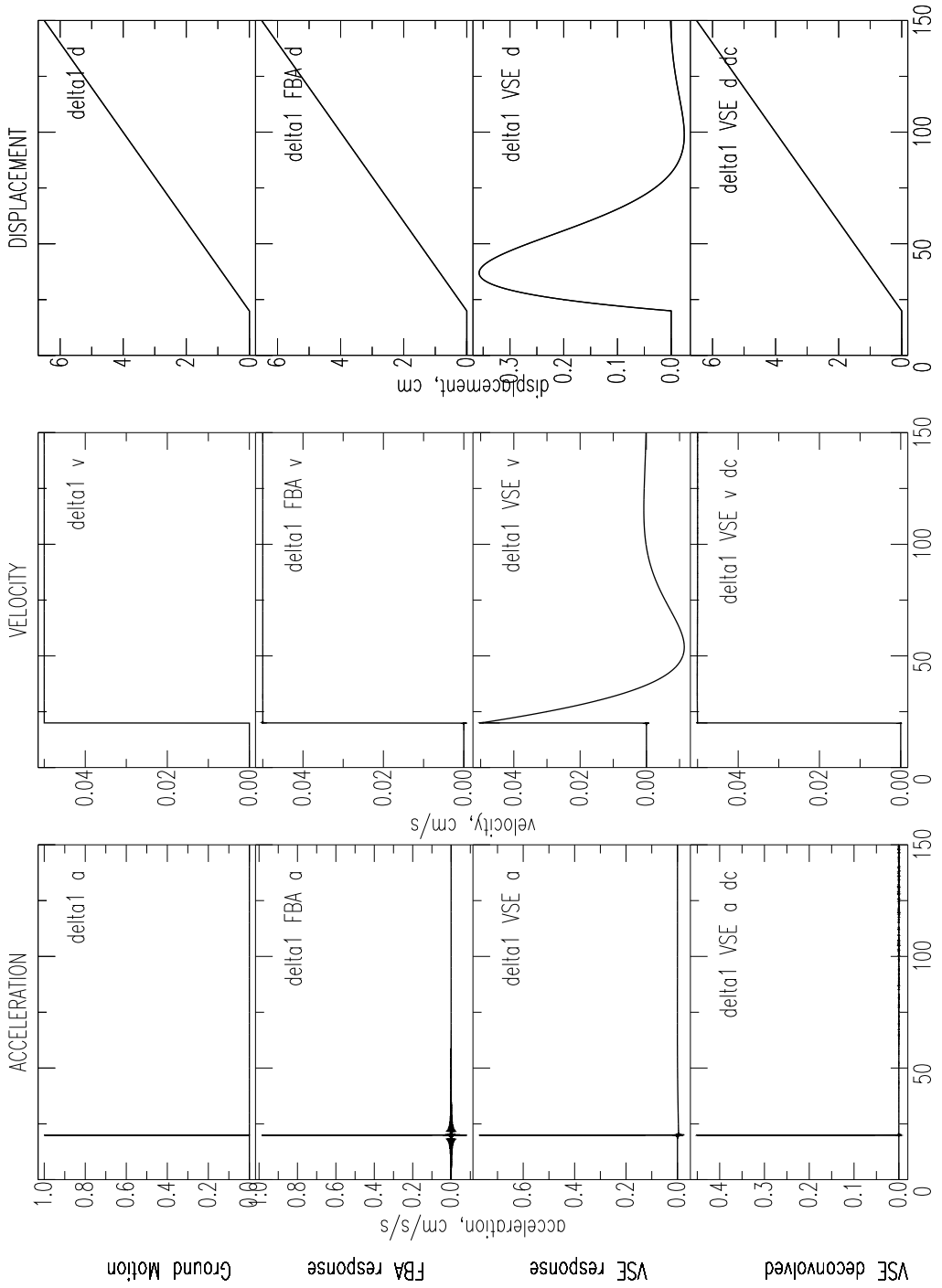

Figure 3.5: Synthetic instrument response to δ-function in acceleration. Typical calibration coil input. Top 3 plots: acceleration, velocity and displacement from input δ-function; 2^{nd}: FBA response; 3^{rd}: VSE response; Bottom: VSE response deconvolved (using direct integration in time domain).

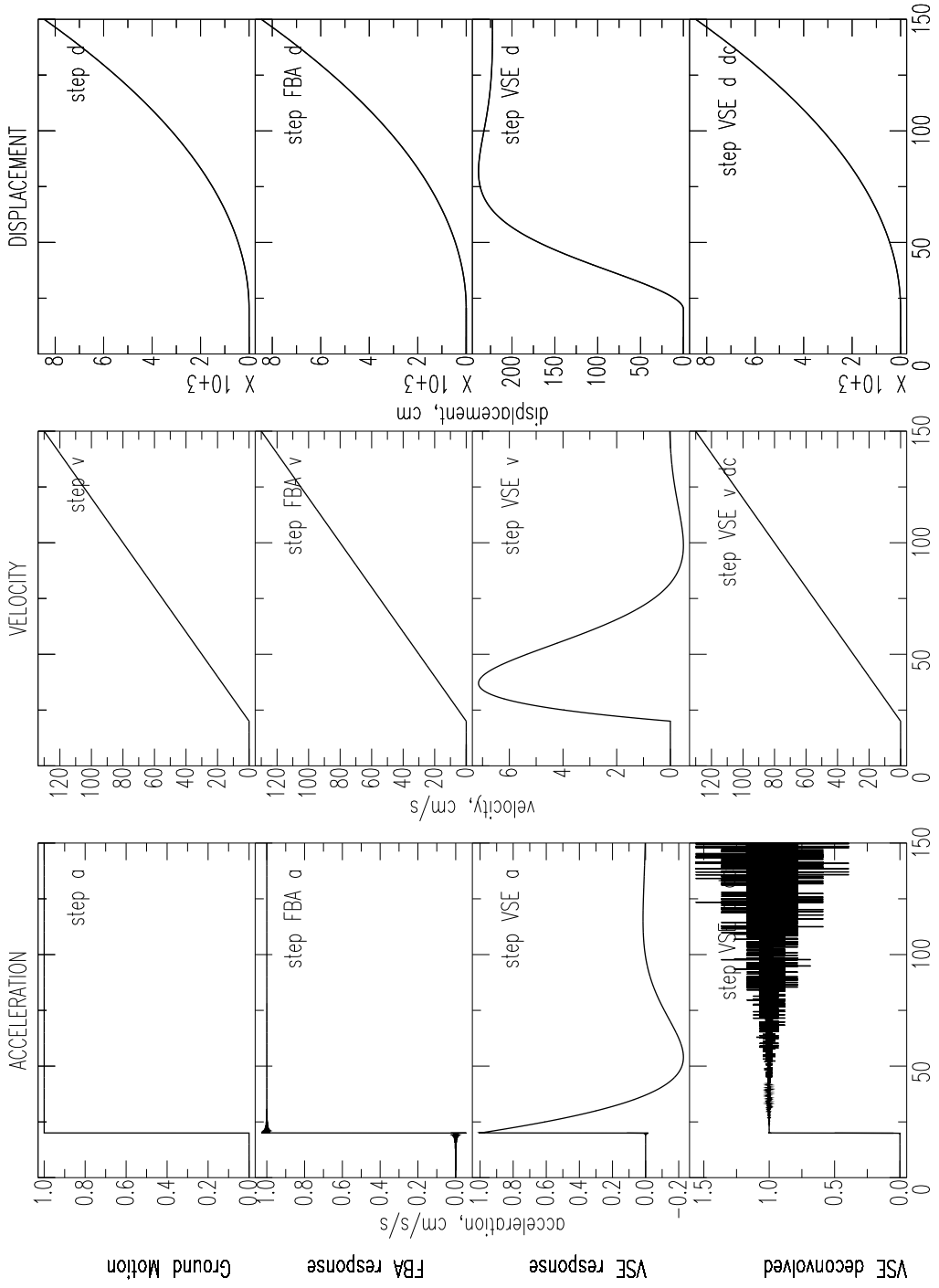

Figure 3.6: Synthetic instrument response to step function in acceleration. Typical calibration coil input, also represents an instantaneous tilting of the ground, or a typical instrument error seen in accelerometers. Top 3 plots: acceleration, velocity and displacement from input step function; 2^{nd}: FBA response; 3^{rd}: VSE response; Bottom: VSE response deconvolved (using direct integration in time domain).

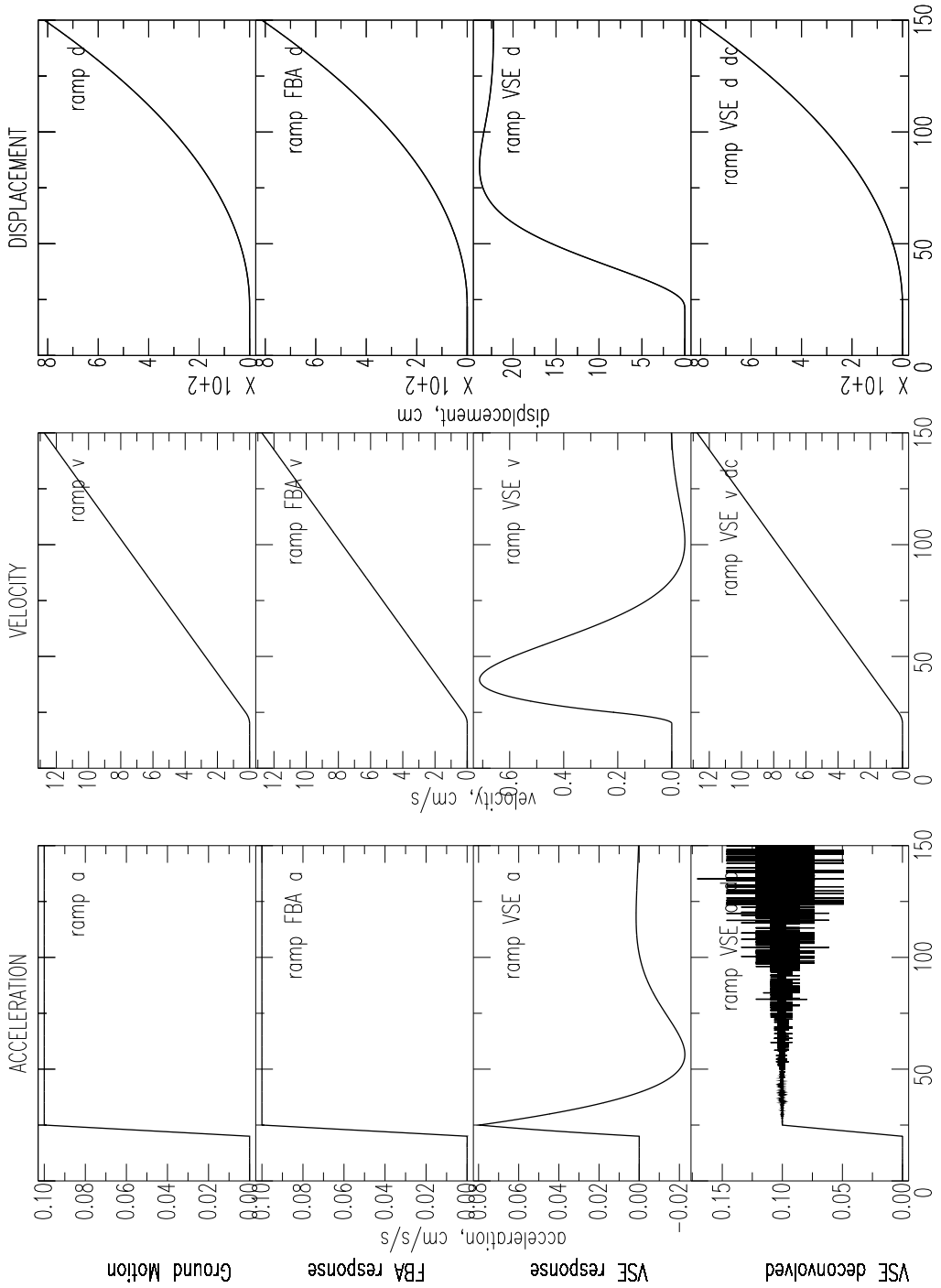

Figure 3.7: Synthetic instrument response to a static offset in acceleration, with 5s ramp. instrument response to a physically more realistic ground tilt. Top 3 plots: acceleration, velocity and displacement from input ramp function; 2^{nd}: FBA response; 3^{rd}: VSE response; Bottom: VSE response deconvolved (using direct integration in time domain). Note this acceleration of $0.1 cm/s^2$ is caused by a tilt of only 0.0058^o ($0.000102 rad$), yet causes over 8m displacement after 130s.

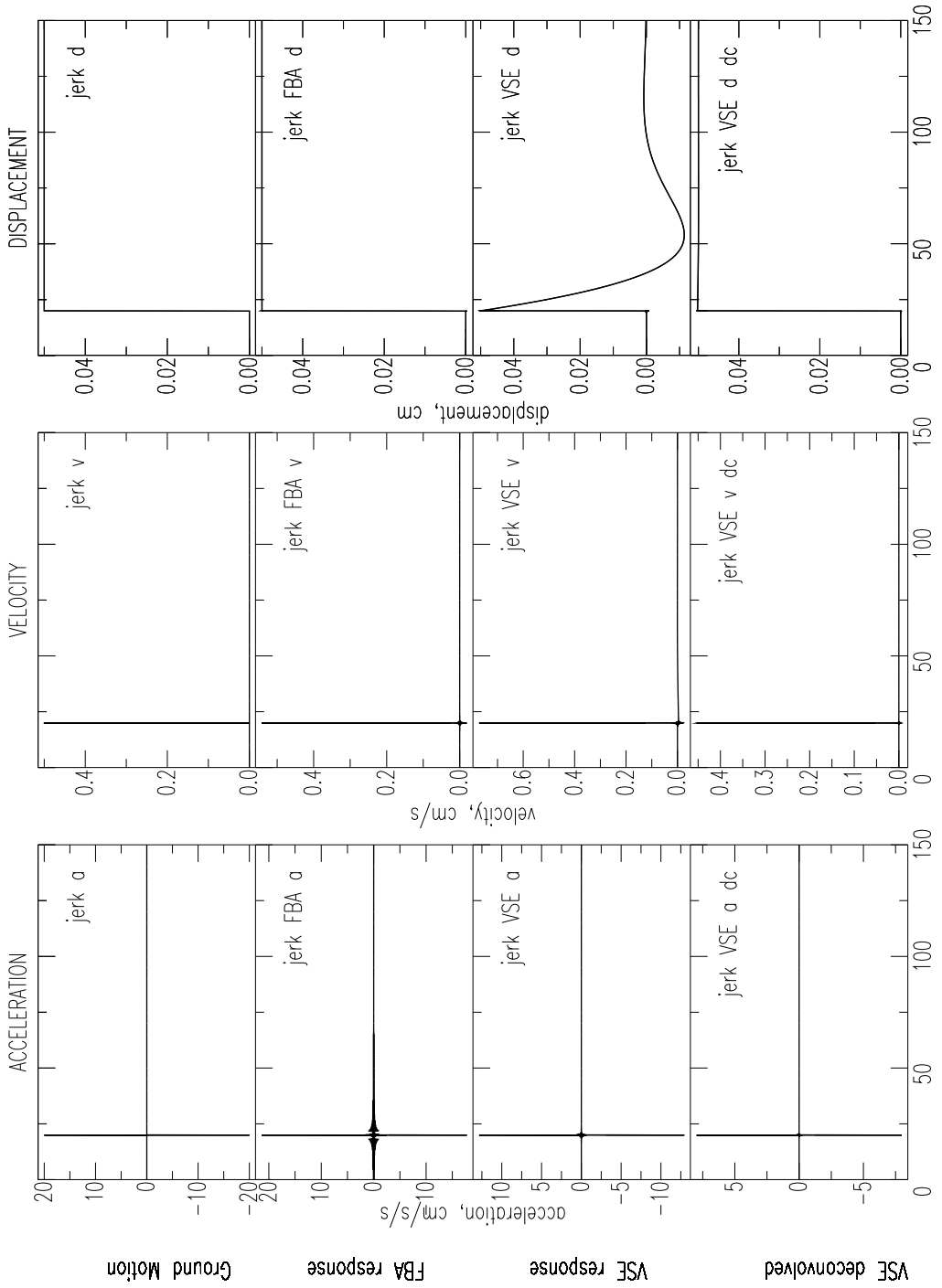

Figure 3.8: Synthetic instrument response to step function in displacement (a 'jerk' in acceleration). Response to a static offset in ground motions. Top 3 plots: acceleration, velocity and displacement from input jerk-function; 2^{nd}: FBA response; 3^{rd}: VSE response; Bottom: VSE response deconvolved (using direct integration in time domain).

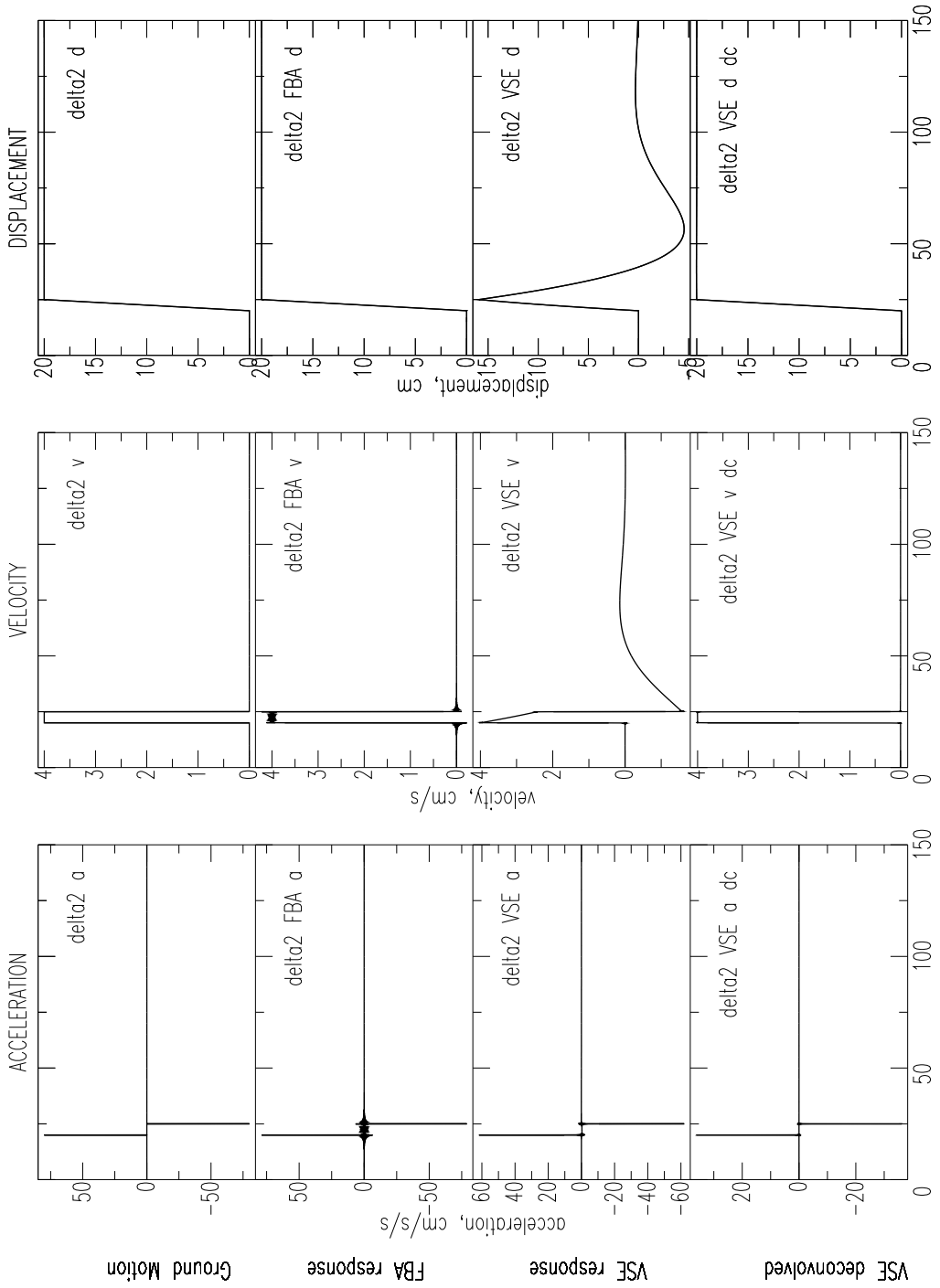

Figure 3.9: Synthetic instrument response to static offset in displacement, with ramp. Physically more realistic than a step in displacement. Top 3 plots: acceleration, velocity and displacement from input function; 2^{nd}: FBA response; 3^{rd}: VSE response; Bottom: VSE response deconvolved (using direct integration in time domain).

6. VSE cart test: displacement of 8m in 10s (*Figure 3.10*). This models a 'perfect' run of the cart test described in this Chapter and Chapter 5. A ramp in velocity from $20s - 22s$ produces a velocity of $1cm/s$, maintained for $8s$ before returning to zero velocity at $30s$, producing a permanent displacement of $8m$ over the $10s$. This produces a simple raw VSE output, but this shape is never recovered in practice, primarily due to tilting over the floor during the displacement.

3.4 Instrument Design and Specifications

The Operation Manual (Tokyo Sokushin Co. Ltd., 2002b) supplied with the instrument reports the following instrument specifications for the VSE-355G2:

$$\begin{aligned}
\textit{frequency range:} &\quad 0.012 \leftrightarrow 70Hz (0.0143 \leftrightarrow 83.3secs) \\
\textit{clip levels:} &\quad \pm 200kine (\pm 2m/s) \\
&\quad \pm 2000gal (\pm 2g, \pm 19.8m/s^2) \\
\textit{sensitivity:} &\quad 100mV/kine, 50mV/kine^2). \\
\textit{maximum output voltage:} &\quad \pm 20V \\
\textit{resolution:} &\quad 10^{-6} gal
\end{aligned}$$

The design of the instrument is described in a document sent through personal communication with the manufacturer (Tokyo Sokushin Co. Ltd., 2002a). The instrument measures velocity as the standard output. The mechanical pendulum is described as having a natural frequency of $3Hz$ and is heavily over-damped, about 10000% of critical, and so the suspension displacement is proportional to ground velocity over a wide frequency band about this free period, from $70Hz$ to $83s$.

The feedback loop is proportional to the displacement of the pendulum, and so the instrument output measures ground velocity within this frequency band. At periods beyond $83s$, the expected response drop-off would be $3dB/octave$, but in earlier models of the instrument, this was found to lead to instabilities with DC offsets, and the VSE-355G2 (and G3) includes an integration circuit in the feedback loop to provide signal drop-off at $6dB/octave$. With such a corner, the instrument may be modeled at long periods as an

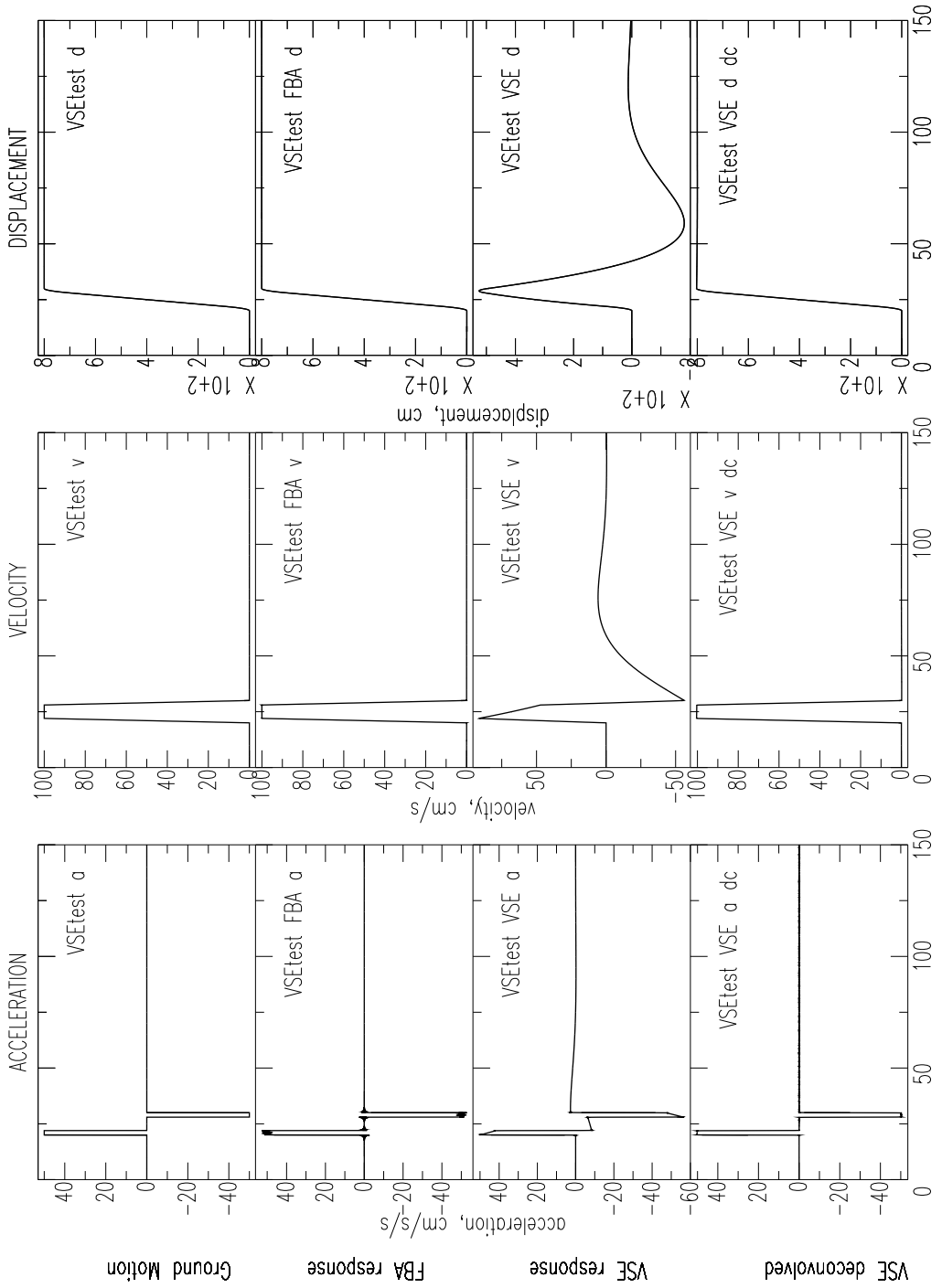

Figure 3.10: Synthetic instrument response to idealised cart test, where a displacement of $8m$ is reached over $10s$ with a constant velocity of $1m/s$. Top 3 plots: acceleration, velocity and displacement from input function; 2^{nd}: FBA response; 3^{rd}: VSE response; Bottom: VSE response deconvolved (using direct integration in time domain).

SDOF with velocity output. This is a similar response to an STS-1 or STS-2. This modeling approximation allows us to determine an equivalent SDOF response for the instrument which is useful in measuring the true long period motion of the ground, deconvolved from the instrument response.

A note on the installation: the horizontal channels had to be interchanged on the VSE-355G2 (and G3, as only components internal to the casing were modified), so N-S output channels actually represent the E-W motion, and vice-versa. This is due to the definition of polarity for the VSE-355G2, which required a clockwise rotation of 90 degrees in order to agree with the standard alignment of other instruments (such as the STS-2 or EpiSensor). In fact this unorthodox polarity is characteristic of all Tokyo-Sokushin products, which is shown in Chapter 4 to cause confusion within seismic networks in Japan - when these instruments are used to investigate static displacements, the results often end up being 90^o or 180^o out of phase with nearby records.

Also, the operational manual supplied by the manufacturer was unclear and insufficient for correct and efficient installation — at least for the English version. Clarification, and indeed correction of the manual required some correspondence with the company and its representatives. Another major source of difficulty involved resolving the pin connections for use with Quanterra dataloggers.

The operation manual does not explicitly state the effective natural frequency of the instrument, nor the effective instrument damping. Both are useful, though not essential, in removing the instrument response in order to recover actual displacements, and correct long period motions beyond about $90s$. One could also use the published Transfer Function, though this is shown to differ from the observed response of the VSE-355G2 instrument, as well as for the modified G3 version.

3.5 Test Data and Analysis

3.5.1 Instrument Sensitivity

The sensitivity of the instrument was determined by comparing data from the VSE-355G2 instrument with data from a Streckeisen STS-2 located on the same pier and recording onto the same $144dB$ Quanterra digitiser.

The instruments were located at Kresge Laboratory, recording onto a Q4128 digitiser, operating as test station PASB in the SCSN. The signals compared were from a small local earthquake, as well as the background noise. The local earthquake was the 16 March 2002 M4.6 event $35.5km$ WNW of Santa Barbara Island, at a distance of $145km$ from PASB. Noise data was taken from a 3hour segment beginning at 08:00 UTC on 16 March 2002.

Records of the raw counts (with mean removed) were band-passed between 0.5–1s for the local earthquake records, and between 5–10s for the noise (measuring the microseisms). In the band-passes described, the time-series were almost identical after multiplication of the VSE records by a scalar constant. For both noise and small earthquake signals, this constant was found to be $\sim$ 150 E-W, $\sim$ 141 N-S and $\sim$ 143 for the Z component. The published STS-2 sensitivity of $15V/cm/s$ is assumed to be correct (quality control for this instrument is generally very high, within 1% of the manufacturer's published sensitivity of $15V/cm/s$). The published VSE-355G2 sensitivity is $100mV/cm/s$, so our expected constant should be 150. For the 3 components there is 0% error E-W, 6% error N-S and 4.5% error in the Vertical component.

Figure 3.11 shows the broadband FFT's of the M4.6 event records for the 3 components, scaled by the above values. The only other processing of the raw counts is to remove the mean of the data.

The Q4128 datalogger gain, G_d, is $40V/2^{24}cts$, equivalent to $419430cts/Volt$. If the Operation Manual sensitivity of $100mV/cm/s$ for the VSE-355G2 sensitivity is assumed to be correct, then the nominal gain is $41,943cts/cm/s$. Similarly, for the STS-2, the sensitivity is $15V/cm/s$, and thus the nominal gain is $6,291,450cts/cm/s$. Subsequent plots in cm/s have been scaled by these gain factors. These values are summarised in Table 3.1.

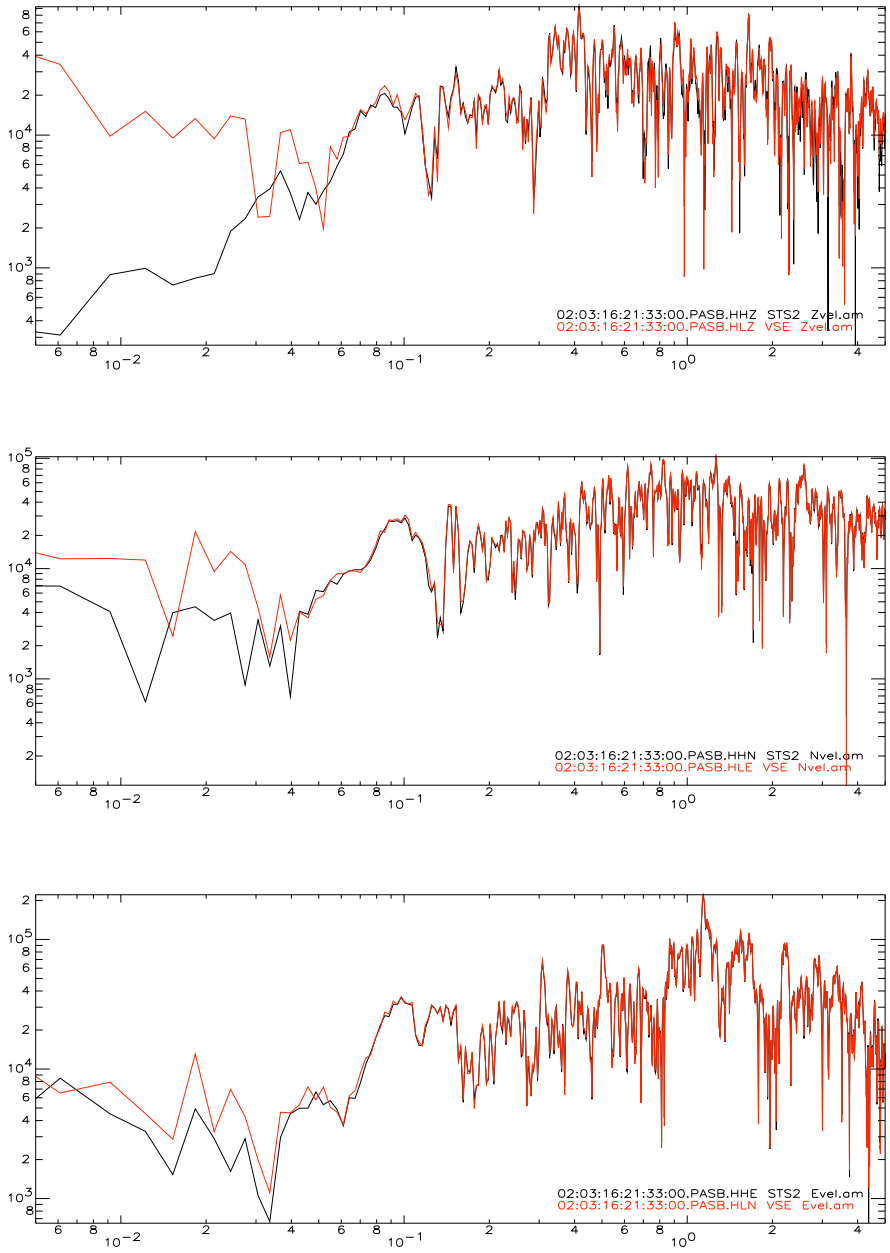

Figure 3.11: Sensitivity scaling: FFT of data recorded at PASB on 03/16/02 for M4.6 event at 145km. Y-axis is FFT of raw counts, X-axis frequency in Hz. Lighter shaded lines are the VSE output in counts multiplied by a sensitivity factor. *(see text on Instrument Sensitivity)*, black is STS-2 output in counts. Top plot is Z, middle is N-S, bottom is E-W component.

3.5.2 Instrument Response

The calibration coil internal to the instrument is used to estimate the equivalent SDOF instrument response at long period. In this test a known current function from a signal generator is applied over the calibration coil, which applies the same function in acceleration to each of the 3 sensors individually.

The SDOF mass displacement response, $G(t)$, to a δ-function in acceleration is:

$$G(t) = \frac{H(t-t_0)}{\omega_d} e^{-\beta(t-t_0)} \sin \omega_d (t-t_0) \tag{3.19}$$

(*Gt* in this case is the same function as described in Equation 3.17 — This solution is observed as the displacement response of the VSE in Figure 3.5.)

$H(t-t_0) =$ *amplitude of a step function at time* t_0 $[\dot{H}(t-t_0) = \delta(t-t_0)]$;

$H = 0$ *if* $t < t_0, H = H$ *if* $t \geq t_0$

where:

$\omega_0 =$ *natural frequency*

$\beta = \omega_0 \zeta, \quad \zeta =$ *damping ratio*

$\omega_d =$ *damped natural frequency* $= \omega_0 \sqrt{1-\zeta^2}$

But as the VSE has a velocity transducer, the output is in velocity. So, the VSE response, $V(t)$ to a δ-function in acceleration is:

$$V(t) = \frac{dG(t)}{dt} = \frac{H(t-t_0)}{\omega_d} [-\beta e^{-\beta(t-t_0)} \sin \omega_d (t-t_0) + \omega_d e^{-\beta(t-t_0)} \cos \omega_d (t-t_0)] \tag{3.20}$$

(This solution is observed as the velocity response of the VSE in Figure 3.5.)

The integral of a δ-function is a step function (which is often the applied current function to a calibration test), the SDOF displacement solution, $D(T)$, to a step input in acceleration is:

$$D(t) = \int G(t) dt = \frac{H(t-t_0)}{\omega_0^2} [1 - e^{-\beta(t-t_0)} \cos \omega_d (t-t_0) - \frac{\beta e^{-\beta(t-t_0)}}{\omega_d} \sin \omega_d (t-t_0)] \tag{3.21}$$

(This solution is observed as the displacement response of the VSE in Figure 3.6.)

So the VSE response to a step function in acceleration is simply $\frac{dD(t)}{dt} = \frac{d[\int G(t)dt]}{dt} = G(t)$, given by Equation 3.19. (This solution is observed as the velocity response of the VSE in Figure 3.6.)

In this case a signal generator was used to apply a step function in Voltage to the calibration, equivalent to a step in acceleration. Thus the raw velocity proportional output should match the shape described by Equation 3.19. The equivalent SDOF response of each of the 3 sensors was estimated by graphically finding the best fit to the VSE-355G2 calibration test output, varying the amplitude and starting time of the step function $H(t–t_0)$, the natural period, $T_0(= 2\pi/\omega_0)$ and damping ζ. The results are shown in Figure 3.12. The top 3 sub-plots of the Figure show the velocity output from the instrument, with the mean of the pre-event noise (in this case the event is the first step) and the gain of $41943 cts/cm/s$ removed from the records. The model is the best fit solution to Eqn. 3.19. The bottom 3 sub-plots are the integral of the velocity output, and the model is the fit to Eqn. 3.21 using the same variables. Note there is permanent offset to this plot, which is inversely proportional to the natural frequency, ω_0.

The natural period of the instrument was found to be $93.2s$ in the East-West component, $93.0s$ in the North-South component for the horizontal sensors, and $94.6s$ for the vertical component. The damping was estimated to be at 65% of critical damping for each of the 3 sensors.

Most subsequent VSE-355G2 data presented in the Chapter now not only will have the gain factor removed, but also have this instrument response removed (using a frequency domain deconvolution).

A comparison of this equivalent instrument response with the published instrument transfer function (Tokyo Sokushin Co. Ltd., 2002a) is in Figure 3.13. There is close correlation between the two, though the actual corner period is longer for the transfer function. The transfer function is:

$$F(i\omega) = \frac{-35 * 10^3}{\left(7007 - \frac{19.46}{\omega^2}\right) + i\left(\omega - \frac{504.4}{\omega}\right)} \qquad [V/m/s] \tag{3.22}$$

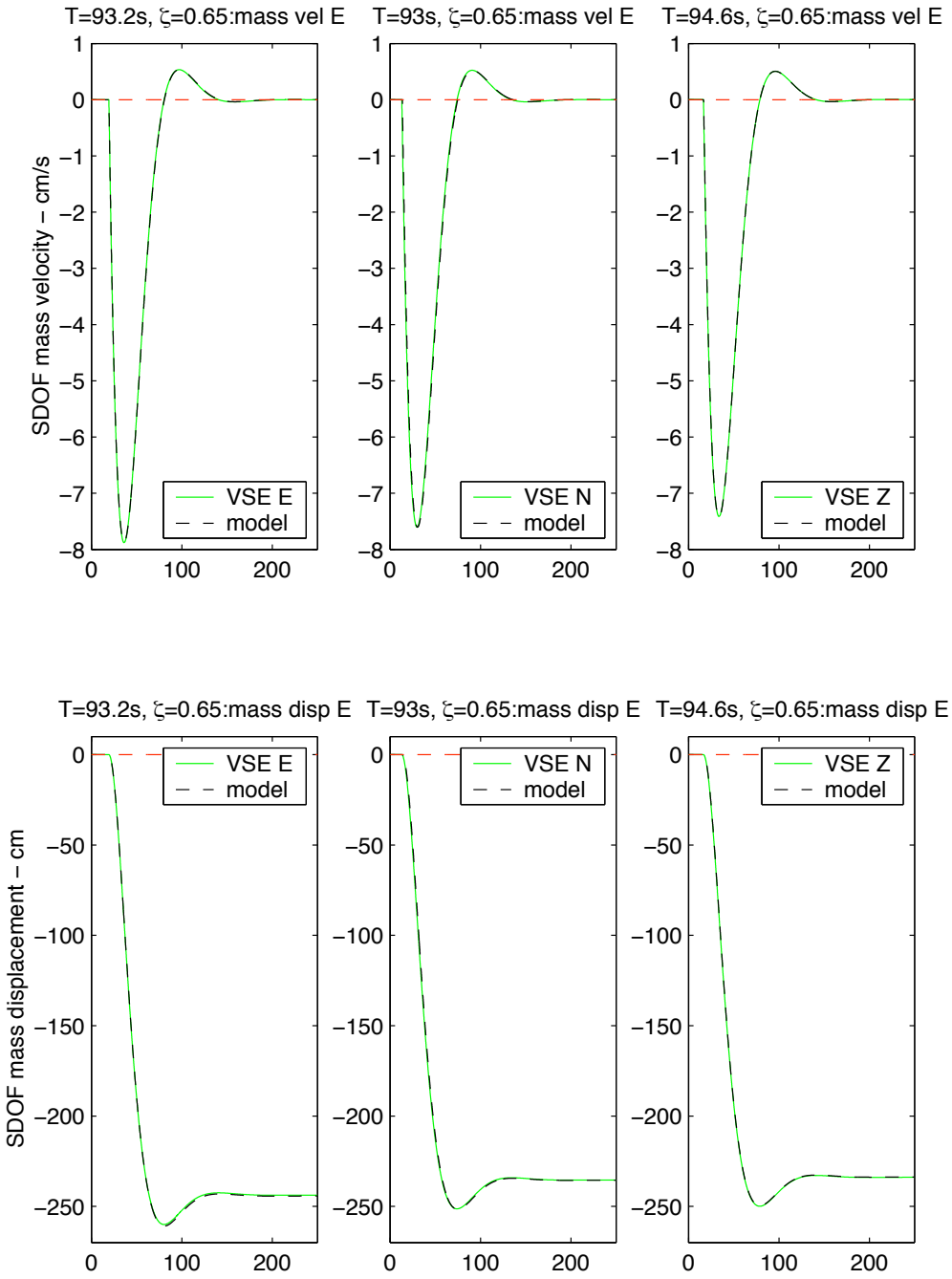

Figure 3.12: Calibration coil response for the VSE-355G2.

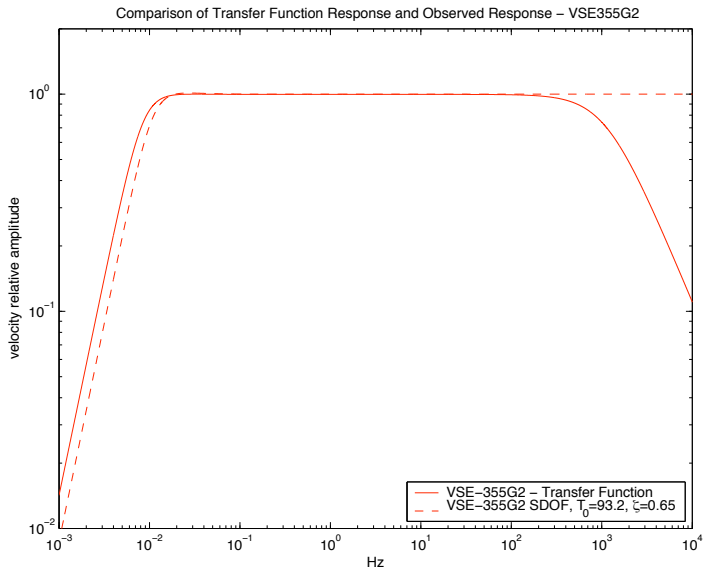

Figure 3.13: Comparison of the theoretical response from the Transfer Function and the observed calibration coil test result.

3.5.3 Instrument Resolution

Figures 3.14, 3.15 and 3.16 show FFT's of ground velocity from co-located VSE-355G2 and STS-2 instruments at PASB, and nearby FBA-23 and STS-1 sensors at PAS, over a 3hour period of noise for the 3 components. The instrument responses have been removed from the records after a bandpass from $0.00125Hz$ — $0.5Hz$ ($2s$ — $800s$).

At periods below $10s$ the VSE-355G2 instrument performs similarly to the STS-1 and STS-2, but above $10s$ through to the instrument corner near $93s$, and out towards $1000s$ the instrument is not capable of resolving the background noise at PAS. At these frequencies, instrument noise saturates the signal at about an order of magnitude higher than the noise at PAS. FBA noise above $10s$ is about 2 orders of magnitude higher than that of the VSE.

In fact in Figure 3.14 the instrument noise of the accelerometer saturates the signal completely over the frequency band here, with no background noise being measured. This noise level is similar for the N-S and Z components, so this instrument data is omitted from Figures 3.15 and 3.16 to remove clutter.

At high frequencies from $1Hz$ — $50Hz$ (see Figure 3.17), a similar lack of resolution for the accelerometer is observed, while the VSE-355G2 instrument noise appears slightly

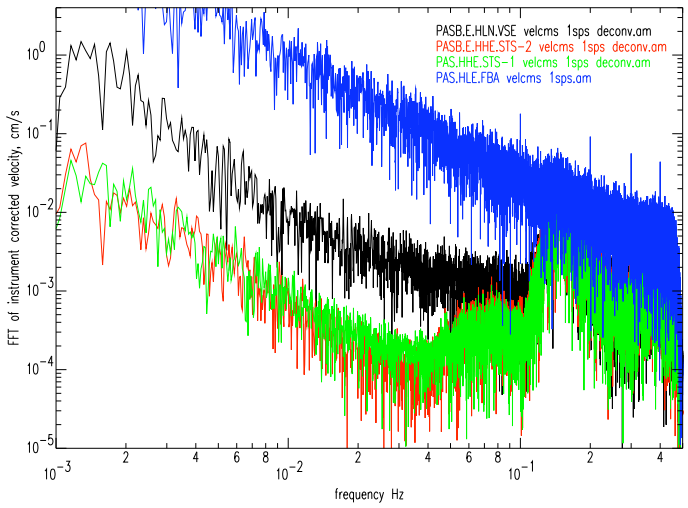

Figure 3.14: Resolution of E-W component. FFT of noise data. The dark trace in the middle is the VSE (PASB), the darker bottom trace is the STS-2 (PASB), and the lighter bottom trace is the STS-1 (PAS). The dark top trace is the FBA-23 (PAS). Instrument response deconvolved.

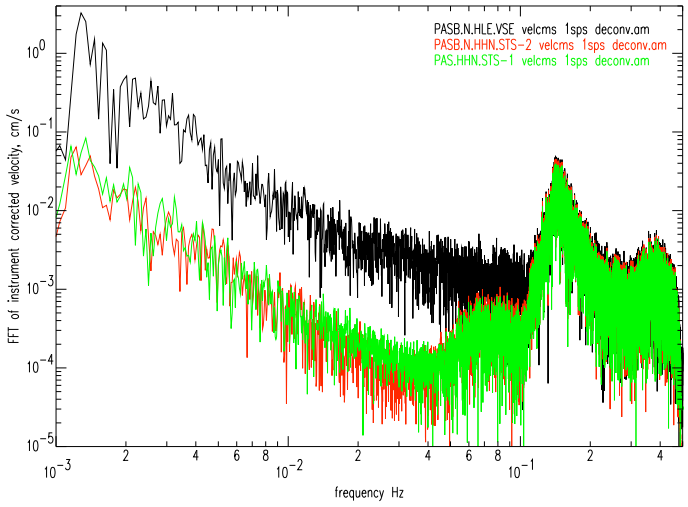

Figure 3.15: Resolution of N-S component — as Figure 3.14.

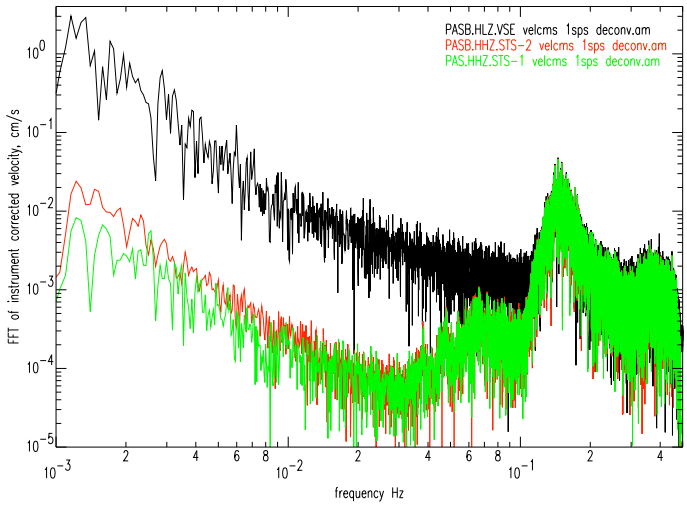

Figure 3.16: Resolution of Z component — as Figure 3.14.

above the background station noise, as seen from the STS-2. The STS-1 response is not sensitive to frequencies above $10Hz$. From Figure 2.10, the FBA is expected to have similar sensitivity to the VSE at about $1Hz$. In Figure 3.17, this is clearly not the case. This is explained by the fact the FBA is not operating well below the $144dB$ assumed in Figure 2.10.

Figure 2.10 presents a frequency-amplitude plot in terms of octave wide band-passes in acceleration. Data from a range of ground motions were plotted along with the band-pass adjusted recording limits of an FBA-23, an STS-2 and a hypothetical strong motion velocity recording device, with limits of $5m/s$ / $5g$ and corner at $120s$ (similar to the VSE-355G2). Figure 3.18 re-presents much of this plot, and includes the additional data presented in this report.

In this Figure 3.18, ground motions recorded on-scale by the FBA-23 lie between the solid red lines. On-scale motions recorded by the hypothetical low-gain broadband seismometer (again similar to the VSE-355G2 analysed in this report) lie between the solid blue lines. The dashed blue lines give the dynamic range of the STS-2. Noise levels are the USGS High and Low Noise Models (Peterson, 1993). The (deconvolved) data discussed in this report are represented by the lines labeled A-D. The dashed red line A is the FBA-23 noise. The dotted-dashed blue line B is the VSE-355G2 noise. The dashed green line C is

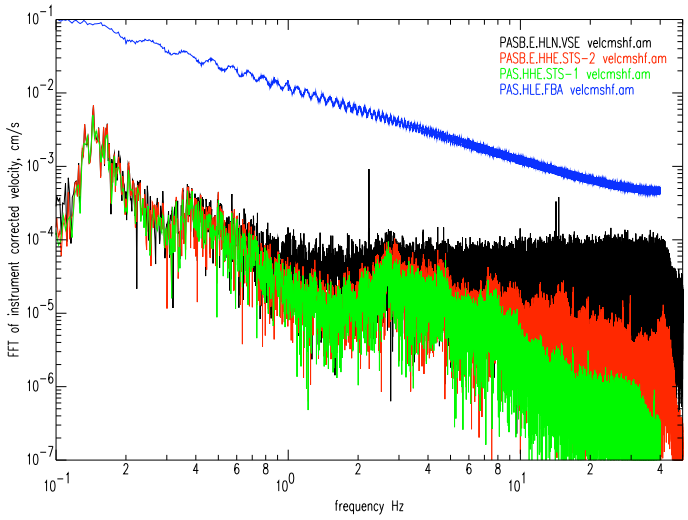

Figure 3.17: Typical resolution of instrument at high-frequency — as Figure 3.14.

the STS-2 noise. The dotted green line D is the STS-1. All this data is from the 3hour time window recorded at Kresge Laboratory. The solid brown line E represents the band-passes from the M7.8 14 November 2001 Qinghai-Xinjiang event recorded by a VSE-355G2 at 38^o in Japan (discussed in Section 3.6).

The VSE-355G2 noise (line B) follows the proposed instrument resolution of the $5m/s$ instrument closely, which indicates the instrument is performing close to the published sensitivities, which corresponds to a dynamic range near $144dB$ if the expected clip was reached (with the clip at $15cm/s$, the instrument is recording at less than $120dB$ dynamic range). The noise attributed to the instrument may also be due to datalogger noise, as this is also at the limit of resolution for the datalogger. At very high frequencies, from $10Hz$ to $50Hz$, the STS-2 records a noise level just below the expected VSE minimum and the actual VSE response is just above this minimum, which reflects the observations in Figure 3.17.

The resolution of the VSE-355G2 is only slightly above the station noise as recorded by the STS-2 and STS-1 (lines C and D, respectively) from $10Hz$ out to about $10s$, and is exactly equal for the microseisms. At longer periods, once again the VSE-355G2 is not able to resolve motions at the noise level of this station.

The FBA-23 represented by line A is not performing at $144dB$ — it is a full order of

magnitude above the expected noise level at $10Hz$, and about a factor of 2 above this level from $10s$ to $1000s$.

Figure 3.19 is a reproduction of a segment of Figure 3.18, and contains only the experimental noise floors from the FBA-23, the VSE-355G2 and the STS-2, along with some Earth signals. The noise from the FBA-23 is nearly 3 orders of magnitude higher ($\sim 60dB$) than the VSE-355G2 at $100s$, and nearly 2 orders higher ($\sim 40dB$) at $10s$. They are equivalent at about $10Hz$. Thus, between $10Hz$ and $1000s$, the region between the dotted red and the dashed-dotted blue lines represents areas of amplitude-frequency space which are recorded by the VSE-355G2 and not by the FBA-23. There is a large portion of teleseismic signals, and also some energy from small local events in this region. This clearly shows the benefit of the VSE-355G2 instrument.

As an aside, it was noted that the dynamic range of the accelerometer at this station was not at its expected level near $140dB$. This warranted a further investigation into the long period response of a collection of accelerometer / datalogger configurations in TriNet/CISN, to determine whether or not this was an isolated occurrence. Three different $3hour$ blocks of noise data were collected for each station, and after octave wide band-passing of the data, the averages are shown in Figure 3.20. this is the same figure as Figure 2.5, where it was used to estimate the average FBA-23 noise floor. PAS / PASB data shown in Figure 3.19 is again reproduced, as the thick dotted lines. Data from stations with an FBA-23 are in black, stations with an EpiSensor are in maroon. This station sample indicates the FBA-23 dynamic range is generally less than $135dB$, whilst the EpiSensor dynamic range is generally closer to $144dB$, and as the published EpiSensor dynamic range is $155dB$, the noise floor may be from the datalogger and not the instrument. The EpiSensor is a better alternative to the FBA-23 for observing teleseismic motions, though it is still significantly noisier than the VSE.

3.5.4 Instrument Clipping

During the VSE-355G2 calibration test it was observed that the applied current would saturate the instrument response at about $600,000cts$, equivalent to $1.43V$ or $14.3cm/s$.

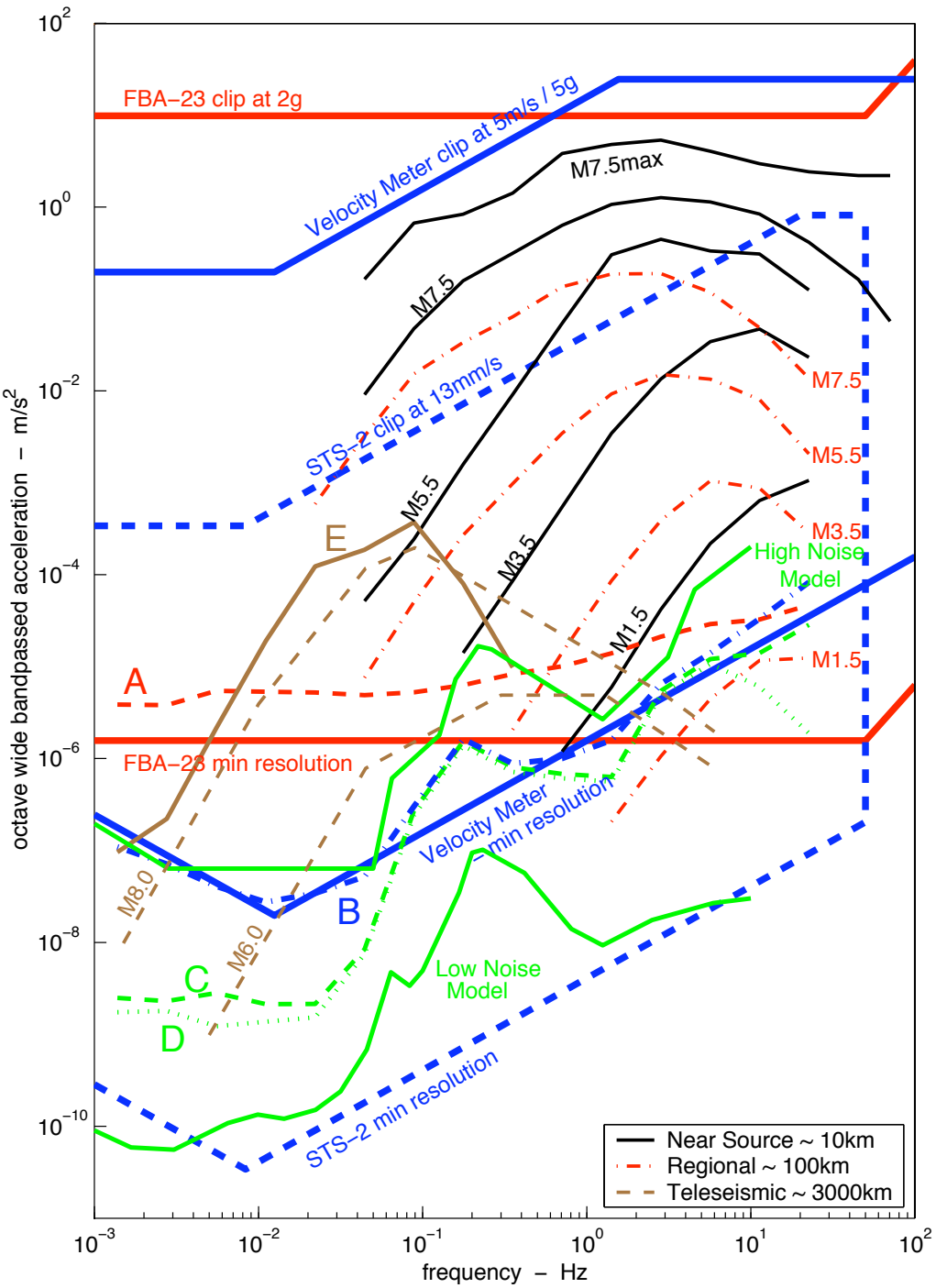

Figure 3.18: Frequency - amplitude plot for octave wide band-passes of ground motion acceleration. Includes typical signals and theoretical instrument limits. Deconvolved noise data from PAS, PASA are represented by lines annotated with letters A-D. A: FBA-23, B: VSE-355G2, C: STS-2, D: STS-1. Line E is teleseismic signal from M7.8 Qinghai recorded on VSE-355G2 in Japan at 4220*km*. (*see text on Instrument Resolution for further explanation.*)

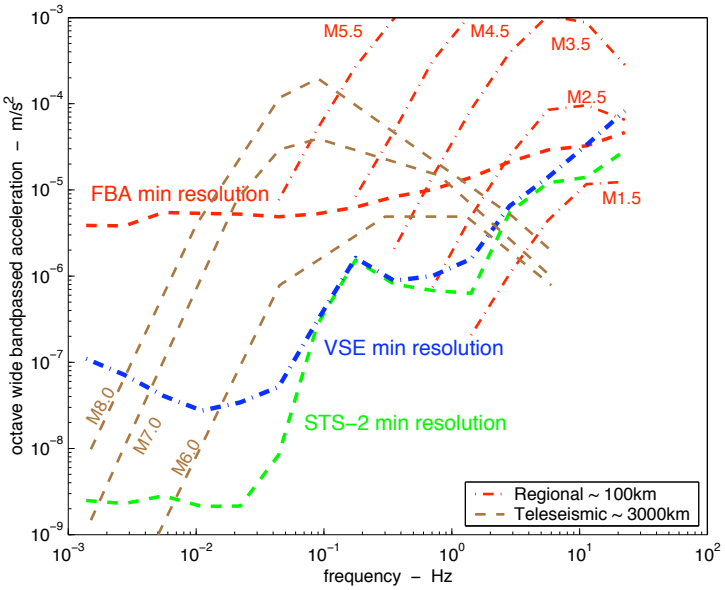

Figure 3.19: Close-up of noise floors of Fig. 3.18, showing minimum sensitivity of instruments at Pasadena.

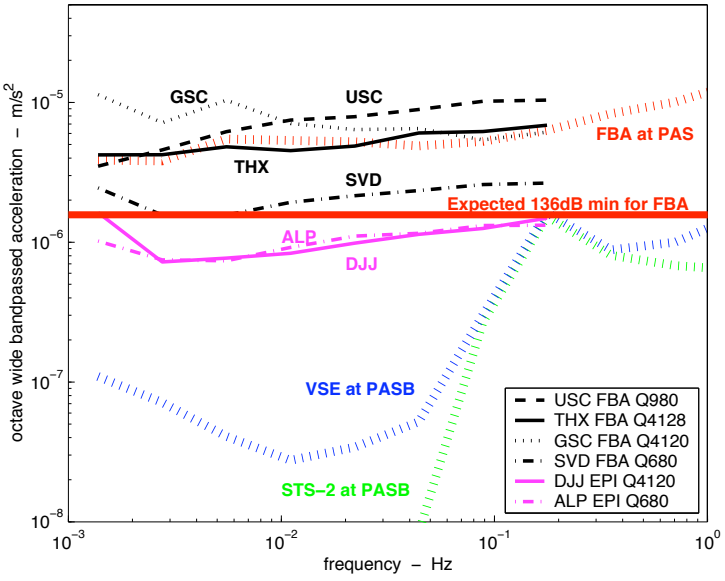

Figure 3.20: Similar to Fig. 3.18. Comparison of noise floors for various accelerometer deployed in TriNet.

This is well below the maximum voltage of $20V$ (or maximum velocity of $2m/s$). In order to get on-scale data for the calibration test, the resistance over the coil was increased until the applied voltage was below this level.

The problem prompted further investigation to confirm whether this was a defect of the instrument or simply a problem confined to the calibration coil. A cart test experiment was developed, in which the instrument would record large velocities of an order seen in strong ground motion records (over $1m/s$). This involved placing the instrument alongside an EpiSensor, both connected to a Quanterra datalogger also on the cart, and robustly moving the apparatus along a laboratory floor (see Figure 3.1 for test layout). The instrument was indeed observed to clip at about $\pm 15cm/s$.

Figure 3.21 illustrates the problem. On this and subsequent plots, the in-plane velocity output from the VSE-355G2 is compared to the in-plane velocity recovered from the EpiSensor. In order to best observe clipping, the VSE output is not deconvolved, and just has the instrument gain removed. Also included in Figure 3.21 are the accelerations recovered from the VSE-355G2 and the EpiSensor. In Figure 3.21, whenever the recorded velocity is greater than about $\pm 15cm/s$, there is a clipping of the VSE. Other differences in the velocity records are attributed to inexact orientation, tilt and differential vibrations on the cart which occur over the course of the test. Accelerations from the EpiSensor are well below $50cm/s^2$ ($5\%g$) and thus the instrument clip level in acceleration ($200\%g$). This is also well below the VSE-355G2 (and G3) clip level in acceleration (at high frequencies, the VSE sensors will clip at $2g$).

The characteristics of the clipping observed in the cart test in Figure 3.21 and during the calibration tests in Figure 3.22 are unlike that of a datalogger clip, where, for the Q4120, the maximum number of counts is reached and the output simply 'flat-lines' until the ground motions return below the datalogger clip level. In these cases, the output will spike above the clip level of about $15cm/s$, but very soon after the excursion will return sharply to the clip level amid some high frequency vibration before resting near $15cm/s$ for a few seconds. For the cart test, the high frequency vibrations cause large acceleration spikes not recorded by the EpiSensor. This behaviour seems to indicate the mechanical seismometer mass has reached its displacement limit and has crashed onto the side rests. This same

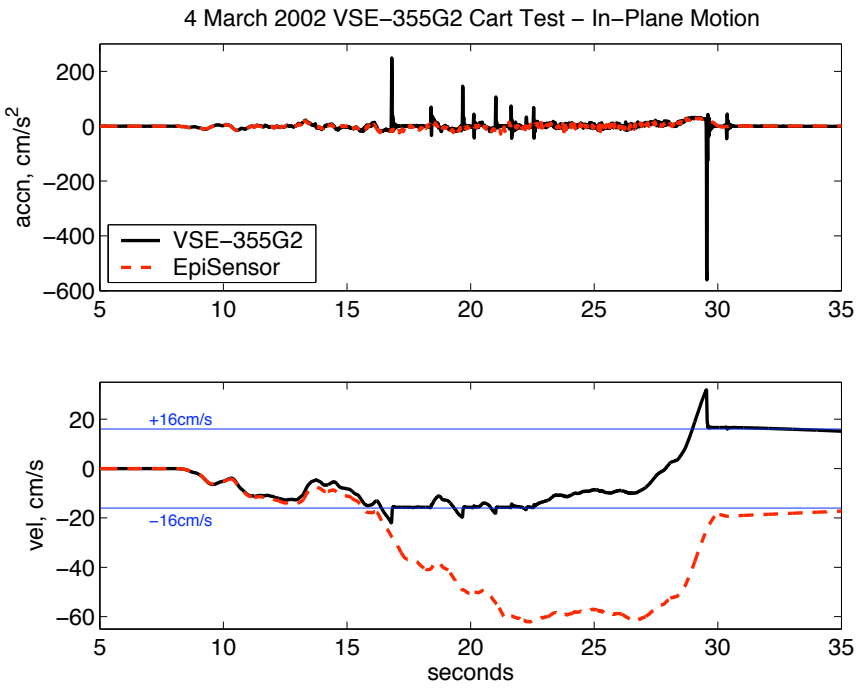

Figure 3.21: VSE and EpiSensor Cart Test results, April 2002. The VSE clips whenever velocities are greater than $\pm 15 cm/s$.

behaviour is observed in the calibration tests with a simple step input (Figure 3.22), where after about $45s$ the velocity would slowly drop back to zero with a shape similar to the step response of the instrument. For the cart test, with a more complicated input, once the actual velocity (as observed in the EpiSensor) changes direction, the instrument returns back on-scale, although of course it records incorrect magnitudes of motion. Any instrument response is drowned out by these subsequent motions. Data presented from strong motions in Chapter 4 show when there are large, high frequency velocity reversals, as is typical of large earthquakes, there is almost no 'resting' at the clip level. Note also that in Figure 3.21, after an initial clip has occurred, if subsequent absolute velocity change exceeds $30 cm/s$, clipping occurs again as the mechanical seismometer appears to hit the opposite side rest due to the peak-to-peak velocity limit being reached. This occurs even though the actual velocity does not appear to have reversed direction.

After correspondence with the manufacturer, the source of the low clipping was identified as a problem with the power regulator, which prevented the final stage amplifier from

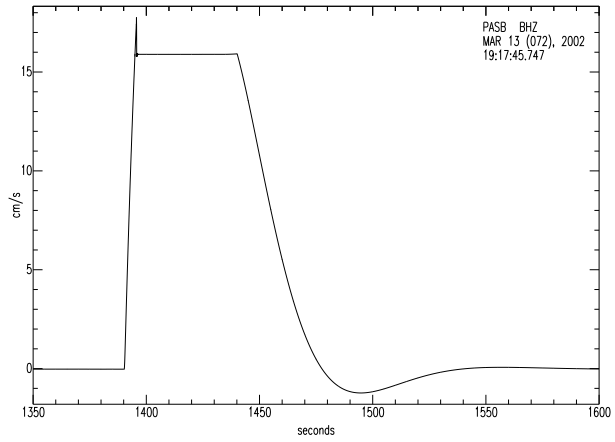

Figure 3.22: Calibration coil test results, March 2002, with clipping above $16cm/s$.

working correctly. The Vice-President of the company, Mr. Isamu Yokoi, visited Caltech on 6/18/02 and 6/19/02 to rectify the problem. Once this problem had been corrected, the cart test was repeated. The test showed improved performance, with good VSE-355G2 correspondence with the EpiSensor data up to 30cm/s (Fig. 3.23). On tests that went above this speed, clipping once again occurred (Fig. 3.24). It is noted that for unknown reasons, the behaviour of the instrument after clipping is different to the previous tests (such as in Fig. 3.21). The clip level here is defined to be at the point where the instrument output departs suddenly and significantly from the accelerometer path, or indeed from its own smooth path. This occurs at about $-50cm/s$ and again at $+30cm/s$, where the VSE seems to spike sharply, then increase linearly with time, until the absolute velocity (as seen from the EpiSensor) begins to decrease. No explanation for this behaviour is presented. Once again, the test is of a robust nature, and the differing longterm trends which appear over the course of the records may be attributed to inexact seismometer orientation or differential tilt during the test.

Initially the manufacturer believed the problems observed in the laboratory at Caltech were isolated to this instrument, and were not representative of all VSE-355G2 instruments. A search of the Japanese Freesia Broadband Seismic Network (F-Net) database in 2001 did not find any recordings with this instrument which had velocities greater than $6cm/s$,

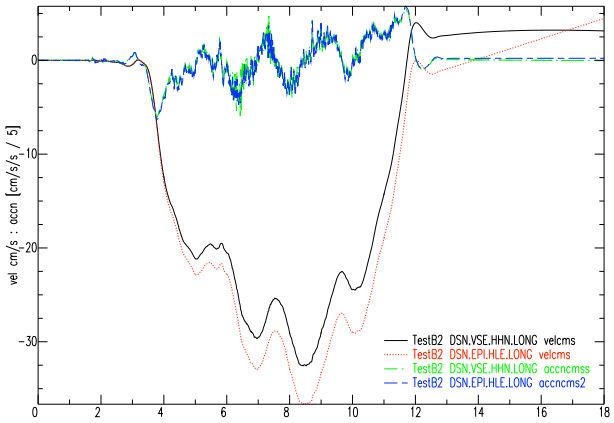

Figure 3.23: VSE and EpiSensor Cart Test results, June 2002. No clipping observed at this speed, below $40cm/s$.

so this could not be independently confirmed. The M8.3 Tokachi-Oki earthquake hit the south-east of Hokkaido Island in Japan on 25 Sept 2003, providing a large set of strong ground motions, with a number of VSE instruments (including the VSE-355G2) within $200km$ of the epicentre. Their performance indicates strange non-linear behaviour above $15cm/s$ is not limited to the model at Caltech. A complete analysis of the performance of the VSE series of instruments during this earthquake is included in Chapter 4.

Following the discovery of the problem, and the initial failure to fully rectify the sensor, a protracted set of visits and correspondence occurred. In mid-2003, an instrument which appeared to satisfy the initial design specifications was tested and deployed within the CISN. Chapter 5 summarises these tests and presents the instrument performance of the VSE-355G3.

3.5.5 Spurious Resonances

FFT's of the noise data collected by the VSE-355G2 indicated the presence of some spurious resonances at frequencies beyond $2Hz$, in all 3 components, as illustrated in Figure 3.25. Data was collected at PASB on 24 March 2002 from 08:00 — 11:00 UTC. These 'spikes' were not observed by the co-located STS-2 or nearby STS-1. Resonances were

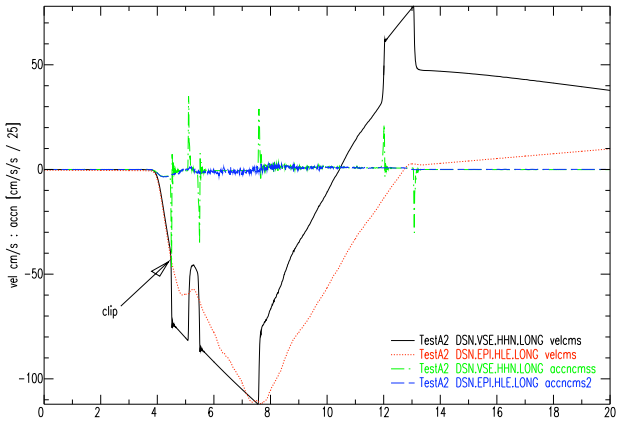

Figure 3.24: VSE and EpiSensor Cart Test results, June 2002. Clipping observed at near 40cm/s, with unexplained linear increase in velocity after clip until true velocity reverses.

observed at 2.225Hz, 14.235Hz and 14.63Hz on the E-W component, 2.225Hz, 12.01Hz and 12.405Hz on the N-S component, and 12.405Hz and 14.63Hz on the vertical component. The very narrow bandwidth of the 'spikes' indicate that if the resonance is due to the mechanical system (and not part of the electronic feedback circuit), it is characterised by very high Q, or low damping.

It is noted these resonances no longer appear in the VSE-355G3 model.

3.6 Recovery of Teleseismic Data

Figures 3.26, 3.27 and 3.28 show the potential of the VSE-355G2 to record long-period motion from giant earthquakes that may saturate the 13mm/s STS-2 even at teleseismic distances. These records are from the 14 November 2001 M7.8 Qinghai-Xinjiang Border Region, China, recorded at Station ZMM, Japan, a distance of 4220km (38°). The maximum velocity is 2mm/s, within 16% of the instrument clip level. The station is part of the Freesia Broadband Seismic Network (F-Net), Japan [`www.fnet.bosai.go.jp`]. In Figure 3.27 we observe the VSE-355G2 is very capable of recording long period motions over 100s for these large events. The FFT in Figure 3.28 indicates this may be valid even out to

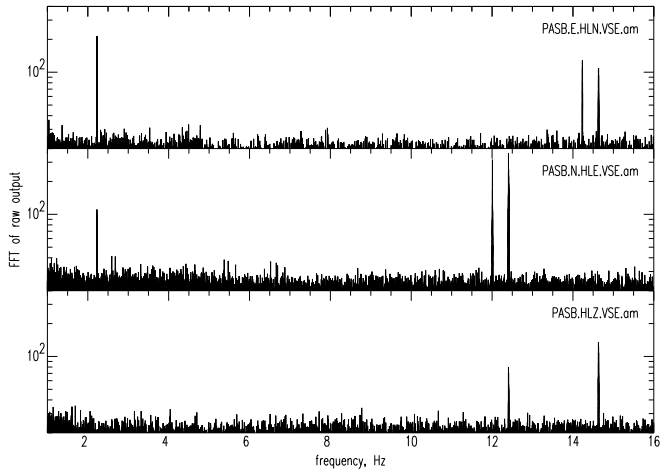

Figure 3.25: FFT of raw VSE-355G2 background noise, indicating presence of spurious resonances.

longer periods. This follows from similar observations made using accelerometer data in Figures 2.12 — 2.14 , though it is noted the accelerometer was not capable of this level of resolution beyond about $50s$.

3.7 Summary

This Chapter documents the investigation into the performance of the tri-axial VSE-355G2 Strong Motion Velocity Seismometer, purchased with IRIS funds in late 2001. The instrument is manufactured by Tokyo Sokushin Co. Ltd. The instrument measures velocity as the standard output, from a heavily over-damped mechanical pendulum and a feedback loop proportional to the pendulum displacement.

The investigation confirms the instrument generally adheres to the manufacturer's specifications, though a very significant problem of a lower than expected clipping level was discovered. As the most critical function of a strong motion seismometer is to record on-scale all ground motions, this is a major flaw. The instrument was observed to produce a highly non-linear response once velocities exceeded $15cm/s$, with high frequency velocity

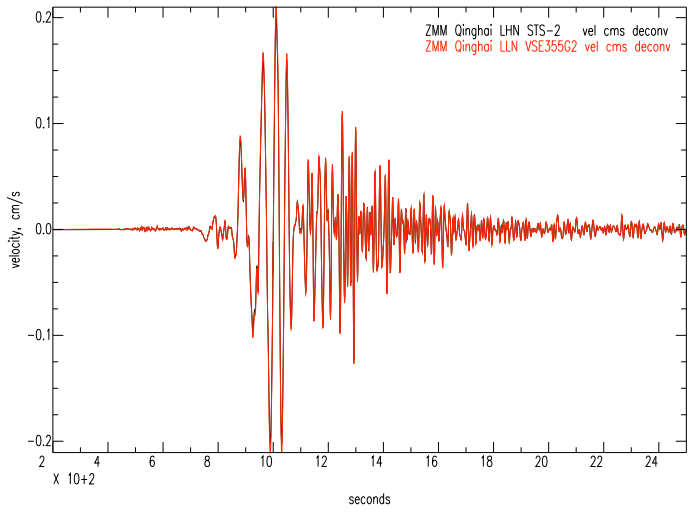

Figure 3.26: Deconvolved (frequency domain) velocity time-series of VSE-355G2 versus co-located STS-2 from Station ZMM recording M7.8 Qinghai, China event, 14 November 2001 at 4221km (38°). Data from the F-Net, Japan.

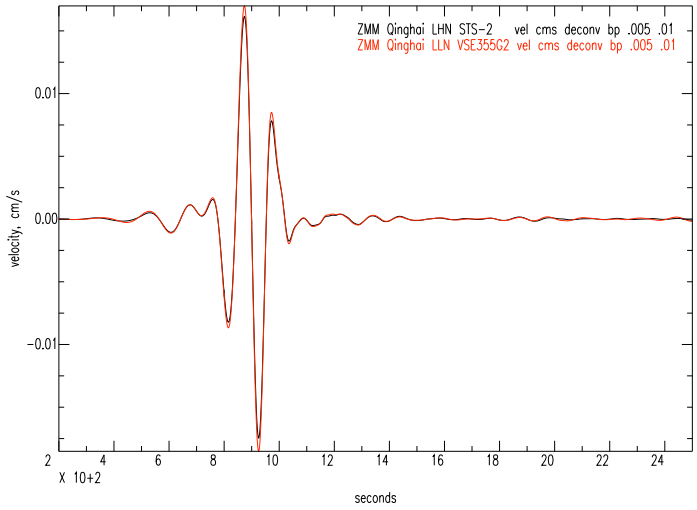

Figure 3.27: Station ZMM, M7.8 Qinghai event: bandpass from 100 to 200s, data is deconvolved (frequency domain).

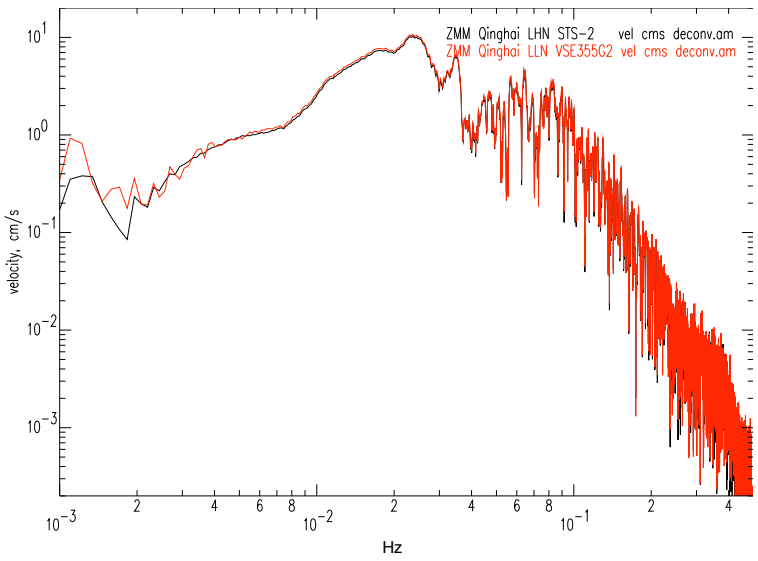

Figure 3.28: Station ZMM, M7.8 Qinghai event: FFT of broadband data, data is deconvolved (frequency domain). Y-axis is FFT of the velocity time-series (cm/s) from Figure 3.26.

jumps preceding a flatline in velocity until a velocity reversal occurred. This is under 5% of the expected clip level of $200 m/s$, and is well below expected, and previously observed, strong motion velocities. The manufacturer produced many fixes to the instrument to rectify the problem, which are discussed in Chapter 5. The new model of the instrument has been renamed the VSE-355G3.

The initial model as delivered, and its predecessor, the VSE-355G, provide the strong motion backbone of the Freesia Broadband Network (F-Net) in Japan, and other Tokyo-Sokushin strong motion velocity instruments are also widely deployed in other Japanese networks. Instrument performance from the M8.3 Hokkaido earthquake is included in Chapter 4.

These initial tests demonstrated the ability of the instrument to resolve long period ($> 30s$) motions was much better than that of a strong motion accelerometer — the instrument had good response even at 100's of seconds. The instrument noise measured at PAS was only slightly above that of the station noise out to $10s$, and remained within an order of magnitude at $100s$ (well over 2 orders of magnitude better than the FBA-23). With the instrument clip at only 5% of $2m/s$, the instrument operated near $120dB$ dynamic range. If

the clip was as expected with this level of sensitivity, the dynamic range would be $144dB$. Instrument sensitivities were within 6% of manufacturer's specifications. All 3 components were approximated as SDOF systems with $T_0 \sim 94s$ and $\zeta = 0.65$.

It is further noted from the investigation that the EpiSensor is a better alternative to the FBA-23 for observing weak regional and teleseismic earthquakes, though it is still significantly noisier than the VSE. For the same 24-bit dataloggers, the FBA-23 dynamic range is generally less than $135dB$, whilst the EpiSensor records closer to $144dB$.